The University of Kitakyushu

Graduate School of Environmental Engineering

Environmental Biosystems

Designing a Novel Vaccine Nanoparticle with β-Glucan and Supermolecular Engineering

β-グルカン工学と超分子工学を用いたワクチンナノメディシンの新規開発

A Doctoral Thesis

by

Noriko Miyamoto

Supervisor: Professor Kazuo Sakurai

March. 2017

Acknowledgements

Table of Contents

Chapter II Crosslinked oligonucleotides(ODN)/ß-1,3-Glucan Nanoparticle through DNA-DNA Hybridization.   36

Chapter III Adjuvant activity enhanced by crosslinked CpG-oligonucleotides in beta-glucan nanogel and its anti-tumor effect 50

Chapter V A two-component micelle with emergent pH
responsiveness by mixing dilauroyl phosphocholine and
deoxycholic acid and its delivery of proteins into the cytosol
96

Proposing a mechanism of the pH responsiveness of DLPC/DA and its

Chapter I

General Introduction

Outline

Immunity is a special form of self-defense found in higher animals. Errors in the immune system are related to a range of diseases. Accordingly, the control of such errors is a possible mode of therapy for diseases. In this chapter, development of cancer vaccines are introduced with these keywords, which are a focus on cancer, immunity, and drug delivery systems (DDSs). In addition, in this thesis, the outline of a CpG/SPG complex for novel cancer vaccination, TAT-ODN/AS-ODN/SPG of cytosol delivery and pH responsiveness lipid micelle for protein delivery to cytosol are explained.

I-1 Cancer Therapy

1.1 Cancer [3]

Cancer is a major public health problem in Japan and around the world. It is the leading cause of death in Japan and elsewhere. The number of cancer patients in Japan is currently 800,000 (Figure 1); this number is increasing and is expected to continue to do so in the future.

1.2 Current state of cancer therapy [3]

Currently, the three major cancer therapies used in a clinical context are radiation therapy, surgical therapy, and chemotherapy. These therapies have shown that cancer is not an incurable disease and have helped those inflicted to survive longer. However, these approaches also have side effects, many of which have yet to be resolved. This is one key area of research for the improvement of cancer treatment. The development of a range of novel cancer therapies is also ongoing. Such therapies are being developed based on interdisciplinary cancer expertise and are enabling improved treatment, widespread prevention, and early detection as never before. These novel therapies include proton therapy, heavy ion radiotherapy, immunotherapy, laparoscopic surgery, and radiofrequency ablation. However, these are not major cancer therapies yet because of their need for advanced equipment and the high cost associated with this. Therefore, a wide range of research on novel cancer therapies is still being undertaken. A lot of cancer patients will be have liberty of cancer therapy options with needs, which are efficacy, cost, combination therapy, and etc., by this diversity cancer therapies.

1.3 Cancer escapes immune surveillance [7,8 9]

Rudolf Virchow (1821–1902), known as the "Father of Pathology", was a 19th
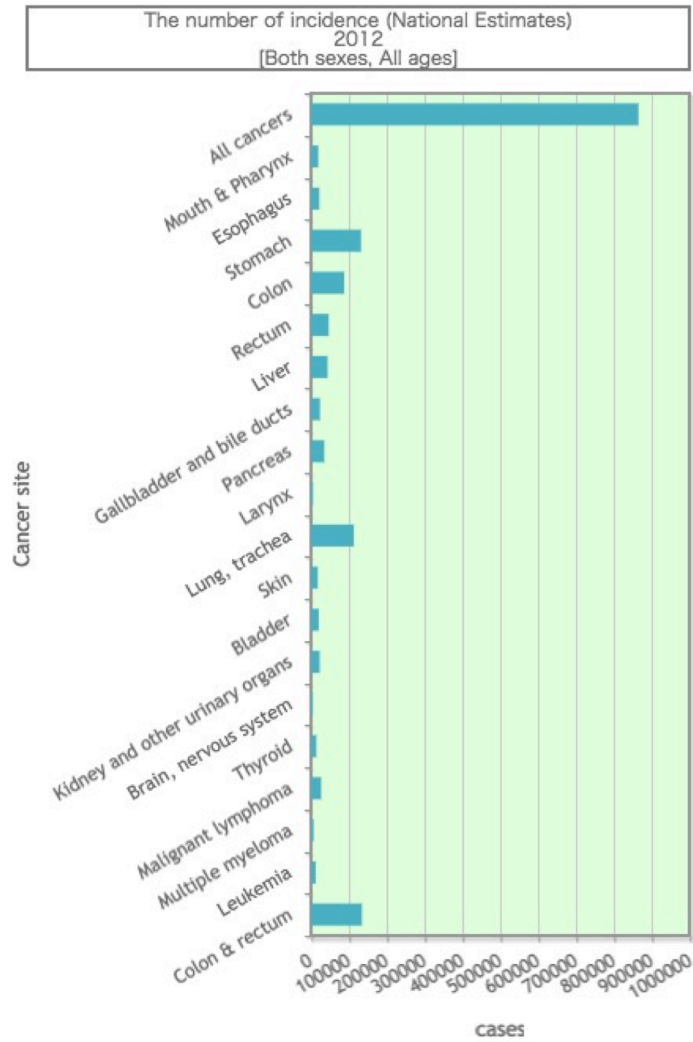
Figure. 1 A number of cancer patients in Japan in 2012 from National cancer center of Japan.

century German pathologist who provided the first indication of a possible link between immunity and cancer. Immunity is divided into two major categories: innate and adaptive immunity. The innate immunity is early response and induces adaptive immunity by antigen presenting. Then the induced adaptive immunity defenses strongly and memorizes immunity. The body's defense against cancer is induced by the presentation of antigens and signaling from components of the innate immune system to the adaptive immune system. However, cancer cells are known to escape immune surveillance by establishing several types of immune suppression (Figure 2).

Tumor cell-intrinsic mechanisms: avoidance of immune recognition and elimination

- Defects in major histocompatibility complex (MHC) class I proteins (e.g., genetic loss of the MHC locus)
- Epigenetic silencing of the antigen processing machinery [e.g., transporter associated with antigen processing (TAP)]
- Loss of tumor-associated antigens (e.g., dedifferentiation of melanoma cells) [10]
- Expression of ligands for inhibitory receptors [e.g., programmed cell death protein 1 ligand 1 (PDL1)]

Tumor cell-extrinsic mechanisms: creation of an immune-suppressive microenvironment

- Infiltration with suppressive cells [e.g., regulatory T cells (Tregs), macrophages, and myeloid-derived suppressor cells (MDSCs)]
- Secretion of immune-suppressive cytokines [e.g., transforming growth factor-β (TGFβ), interleukin-10 (IL-10), and vascular endothelial growth factor (VEGF)]

Immunotherapy is one novel cancer therapy that works by limiting the escape from immune surveillance by these above mechanisms. Breakthroughs in immunotherapy have been achieved via the use of checkpoint inhibitors, chimeric antigen receptor (CAR), T-cell therapy, and cancer vaccine (Figure 3). Remarkable progress in treating cancer has recently been achieved via these immunotherapies. In the near future, immunotherapy should become one of the major forms of cancer therapy.
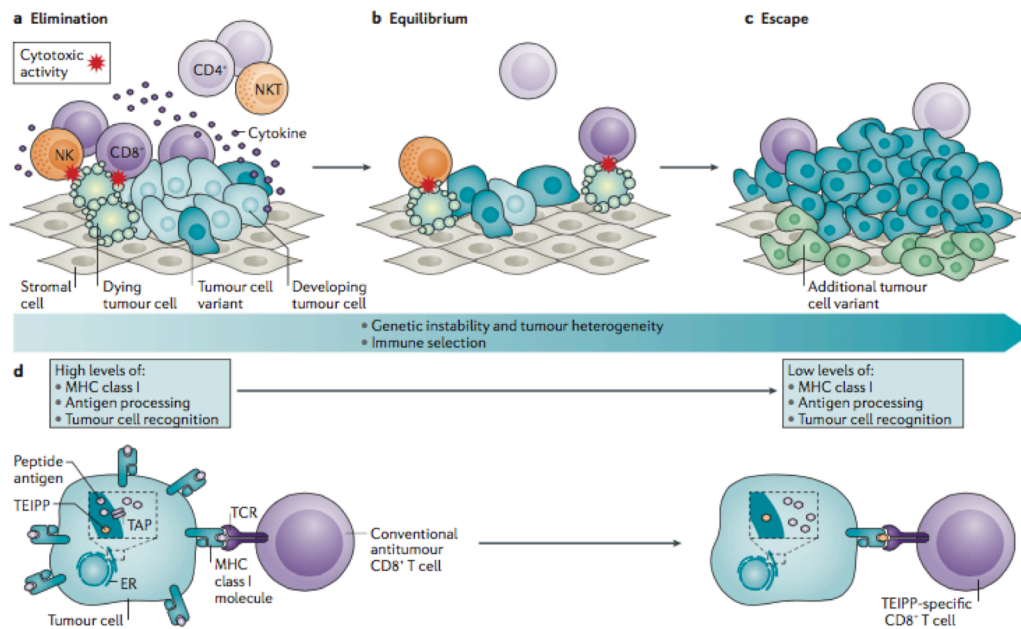
Figure. 2 Tumor escape gives rise to alternative peptide antigens. The three phases of cancer immune-editing.

Cancer describe the intricate relationship between a tumor and its infiltrating immune system, during which genetic instability and tumor heterogeneity increase and immune selection of tumor cell variants occurs. In the first phase (part a), the immune system is in control, which results in the elimination of tumor cells. In the second phase (part b), tumor cell variants arise that have increasing capacity to survive immune attack, such that in the third phase (part c), the tumor escapes immune control and additional tumor cell variants develop. The escape phase is characterized by a multitude of tumor-intrinsic mechanisms that enable the tumor to avoid immune recognition, as well as tumor-extrinsic mechanisms that result in active immune suppression in the microenvironment. During the first phase, tumor cells generally express high cell-surface levels of major histocompatibility complex (MHC) class I, their antigen processing machinery (APM) is still intact and they are easily recognized by CD8+ T cells that are specific for conventional tumor antigens (part d). In the later phases, tumor cells show a decrease in the cell-surface levels of MHC class I that is often associated with less antigen presentation owing to APM defects; thus, there is reduced recognition and eradication of tumor cells by CD8+ T cells specific for conventional tumor antigens. However, a new set of tumor antigens arises; these are known as T cell epitopes associated with impaired peptide processing (TEIPP) and constitute alternative peptides that are uniquely presented by tumors in the escape phase. The copyright is owned by the Nature Publishing Group, from which permission to reproduce this figure was obtained [5]

I-2 Cancer Vaccination

1.1 Vaccines

The work of Edward Jenner (1749–1823), the first to develop a vaccine based on immune mechanisms, benefited the human race tremendously. Vaccines activate self-defense with innate to adaptive immunity by using non-self-antigens such as bacteria and viruses and exhibits various functions depending on the type of antigen.

1.2 Cancer vaccinations [1,11]

Generally, tumor antigens are classified into two categories: (1) tumor-associate antigens (TAAs), which are overexpressed in tumor cells compared with their level in normal cells; and (2) tumor-specific antigens (TSAs), which are expressed only in tumor cells. TSAs are much less well defined and little is known about them. One potential option for treating cancers is to administer an artificially designed antigen [11], such as a synthetic antigenic peptide or protein, for cancer vaccination.

Although many pre-clinical and clinical trials of cancer vaccines have been undertaken since the mid-1990s [12,13], most of them failed to reach a level of efficacy for clinical application, in contrast to other cancer therapies, and for immune escape mechanisms. One major cause of this failure was an inability to induce significant immune responses because of the lack of an appropriate adjuvant and delivery carrier to a responsive immunocyte [14].

1.3 Cancer adjuvants [4,15]

Adjuvants are introduced exogenous substances, when combined with an antigen, enhance antigenicity and elicit the desired immune response. To inhibit immune escape and cancer growth, it is necessary to control the immune system not only by using a

14

suitable antigen for a cancer vaccine, but also by introducing an appropriate adjuvant. The external factors pathogen-associated molecular patterns (PAMPs) activate innate immunity to induce adaptive immunity through pattern recognition receptors (PRRs) (Figure 3). PAMPs have been developed as an adjuvant, shown to be efficacious for several vaccines, and entered into clinical trials (Table 1). When developing an adjuvant, the necessary features include a lack of side effects, efficacy, low cost, and cleary immunity mechanisms.
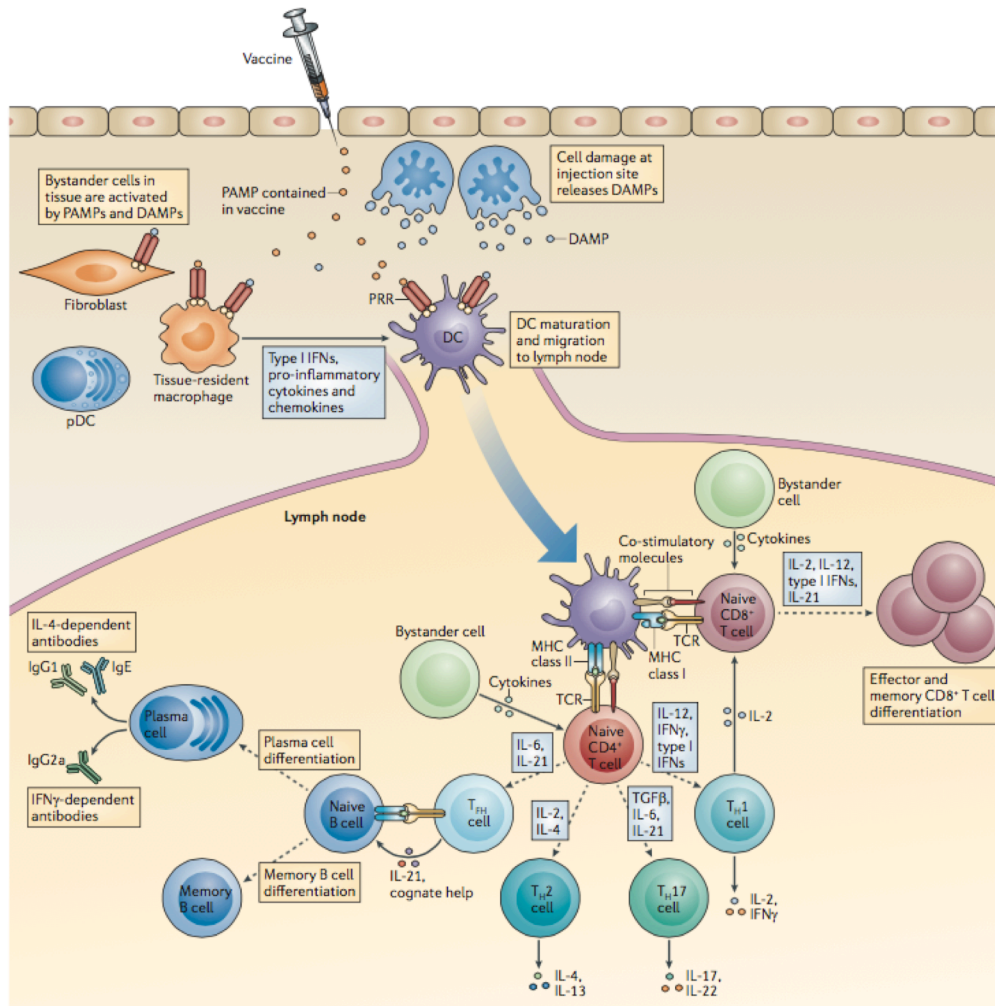
Figure. 3 Induction of adaptive immune responses to vaccines through PRR-mediated dendritic cell activation.

Vaccines may contain pathogen-associated molecular patterns (PAMPs) or may induce the local release of damage-associated molecular patterns (DAMPs). These PAMPs and DAMPs are detected directly by pattern-recognition receptors (PRRs) expressed by dendritic cells (DCs), leading to DC activation, maturation and migration to the lymph nodes. Alternatively, PRR-mediated recognition of PAMPs and DAMPs by bystander cells may induce the release of tissue-derived factors, such as cytokines, that may cooperate in the activation and orientation of the DC response. In the lymph nodes, the activated DCs may present antigens to T cells, provide them with co-stimulatory signals and stimulate their differentiation by providing a favorable cytokine milieu. The copyright is owned by the Nature Publishing Group, from which permission to reproduce this figure was obtained [4].

16

Table. 1 Active immunotherapies in phase III development. The copyright is owned by the Nature Publishing Group, from which permission to reproduce this table was obtained [1].

Immunotherapy	Targeted antigens	Adjuvants/immune modulators	Study population	n	Outcomes	References
Prostate cancer						
Autologous cell vaccine: sipuleucel-T, Provenge®	PAP	GM-CSF	Metastatic, castration-resistant prostate cancer	512	OS: 25.8 months vs 21.7 months (HR 0.78; $P=0.03$) PFS: 3.7 months vs 3.6 months (HR 0.95; $P=0.63$) T-cell response in 73.0% vs 12.1% of patients	50–55
Allogeneic tumour cell vaccine: GVAX	Tumour cell	GM-CSF	Castration-resistant prostate cancer	626	OS: 20.7 months vs 21.7 months with docetaxel plus prednisone (HR 1.03; $P=0.78$)‡	70, 194
Allogeneic tumour cell vaccine: GVAX	Tumour cell	GM-CSF	Castration-resistant prostate cancer	408	OS: 12.2 months in combination with docetaxel vs 14.1 months docetaxel plus prednisone (HR 1.70; $P=0.0076$)§	71, 195
Breast cancer						
Peptide vaccine: Theratope	Sialyl-Tn	KLH	Metastatic breast cancer, in remission after first-line chemotherapy	1,028	Median OS: 23.1 months vs 22.3 months ($P=0.916$) With concomitant endocrine therapy, OS: 39.6 months vs 25.4 months ($P=0.005$) Median TTP: 3.4 months vs 3.0 months ($P=0.353$) With concomitant endocrine therapy: 10.6 months vs 6.3 months ($P=0.078$)	76, 77
Lung cancer						
Peptide vaccine: tecemotide (L-BLP25)	MUC1	Liposomal monophosphoryl lipid A plus cyclophosphamide	Unresectable stage III NSCLC; after chemo-radiotherapy	1,239	Median OS: 25.6 months vs 22.3 months (HR 0.88; $P=0.123$); OS with concurrent chemotherapy: 30.8 months vs 20.6 months (HR 0.78; $P=0.016$); OS with sequential chemotherapy: 19.4 months vs 24.6 months (HR 1.12; $P=0.38$)	79–81, 197
Peptide vaccine: GSK1572932A	MAGE-A3	Liposomal AS15	Completely resected stage IB–II NSCLC	182	Trial terminated owing to failure to meet primary end points of extended DFS. Not possible to identify gene signature predicting benefit	85, 86
Allogeneic tumour cell vaccine: belagenpumatucel-L, Lucanix™	Tumour cell	Anti-TGF-β	Stage IIIB–IV NSCLC	532	Median OS: 20.3 months vs 17 months (HR 0.94; $P=0.594$) Non-adenocarcinoma: 19.9 months vs 12.3 months (HR 0.55; $P=0.036$)	93, 198
Melanoma						
Peptide vaccine	gp100	IL2 plus Montanide™ ISA51	Locally-advanced stage III or stage IV melanoma	185	OS: 17.8 months vs 11.1 months ($P=0.06$) PFS: 2.2 months vs 1.6 months ($P=0.08$) T-cell responses in 7 of 37 (19%) patients Higher levels of CD4⁺foxp3⁺ cells in patients with clinical response ($P=0.01$)	35, 198
Peptide vaccine: GSK 2132231A	MAGE-A3	QS-21	Resected melanoma	1,349	Failed to meet primary end point of DFS; ongoing for end point of DFS in patients with predictive gene signature	100
Pancreatic cancer						
Peptide vaccine: GV1001	Telomerase	GM-CSF	Locally-advanced and/or metastatic pancreatic cancer	1,062	OS: 8.4 months (concurrent with chemotherapy) and 6.9 months (sequential chemotherapy) vs 7.9 months with chemotherapy alone (NS)	113, 199, 200
Colorectal cancer						
Autologous tumour cell vaccine: OncoVAX®	Tumour cell	BCG	Resected stage II–III colon cancer; after resection	254	42% reduction in the risk of recurrence and/or death ($P=0.032$); greatest effect in stage II disease with 60% reduction in risk of recurrence and/or death ($P=0.007$) and 54% reduction in risk of death	121
Haematological malignancies						
Autologous anti-idiotype vaccine	Idiotype	KLH	Advanced follicular lymphoma, with complete response after chemotherapy	177	PFS: 23.0 months vs 20.6 months ($P=0.256$) ≥1 blinded vaccination: 44.2 months vs 30.6 months ($P=0.047$)	130, 201

*Trials listed on Clinicaltrials.gov website; accessed on 19th September 2013. Survival data are medians and comparisons are for active treatment versus placebo or control, unless otherwise stated. ‡Study terminated early following futility analysis. §Study terminated early owing to excessive death in vaccine arm. Abbreviations: BCG, bacillus Calmette-Guérin; DFS, disease-free survival; GM-CSF, granulocyte-macrophage colony-stimulating factor; gp100, glycoprotein 100; HR, hazard ratio; KLH, keyhole limpet haemocyanin; L-BLP25, BLP25 liposome vaccine; MAGE-A3, melanoma-associated antigen 3; MUC1, mucin-1; n, number of patients; NS, not significant; NSCLC, non-small cell lung cancer; OS, overall survival; PAP, prostatic acid phosphatase; PFS, progression-free survival; QS-21, a plant extract derived from Quillaja saponaria that enhances the immune responses to antigens targeted by vaccines; RT, radiotherapy; TGF-β2, transforming growth factor β2; TTP, time to progression; vs, versus.

I-3 Drug Delivery Systems and Cancer Vaccines

1.1 Drug delivery systems

The German Nobel laureate Paul Ehrlich (1854–1915) introduced the concept of "magic bullets" for efficacy drug delivery more than 100 years ago [16]. This concept is first generation of drug delivery systems (DDSs), which have research widely at recent. Figure 4 shows several nanocarriers in nanotherapeutic platforms. Nanocarriers are excellent for drug delivery as they contribute multiple functions. The design of nanocarriers, including their morphology, size, and chemical surface, plays a significant role in their cellular uptake and targeting site (Figure 5) [6]. Therefore, the functionality of carriers is important for efficacy. (e.g. Responsible pH and enzyme)

For the medical application of a DDS, it is important to fulfill the criteria set by drug administration agencies. This refers not only to efficacy, pharmacokinetics, and safety profiles but also to prove clearly chemical, physical factors, and their measuring techniques based on materials.

1.2 Cancer vaccinations and DDSs [5,6]

Nanocarrier design for effective cancer vaccines requires the ability to overcome relevant tissue barriers and efficiently deliver an antigen with an adjuvant to antigen-presenting cells (APCs). Then, APCs can induce cytotoxic T lymphocytes (CTLs) at lymph nodes by presenting the antigen to them along with co-signals. Recently, several groups have expanded upon the size-based targeting strategy of nanocarriers to also incorporate specific ligands to promote vaccine particle capture by specific cell types in lymph nodes. We believe that cancer vaccination with a DDS, which is highly efficacious and enables complete recovery from cancer, will soon provide a successful option for cancer therapy.

18
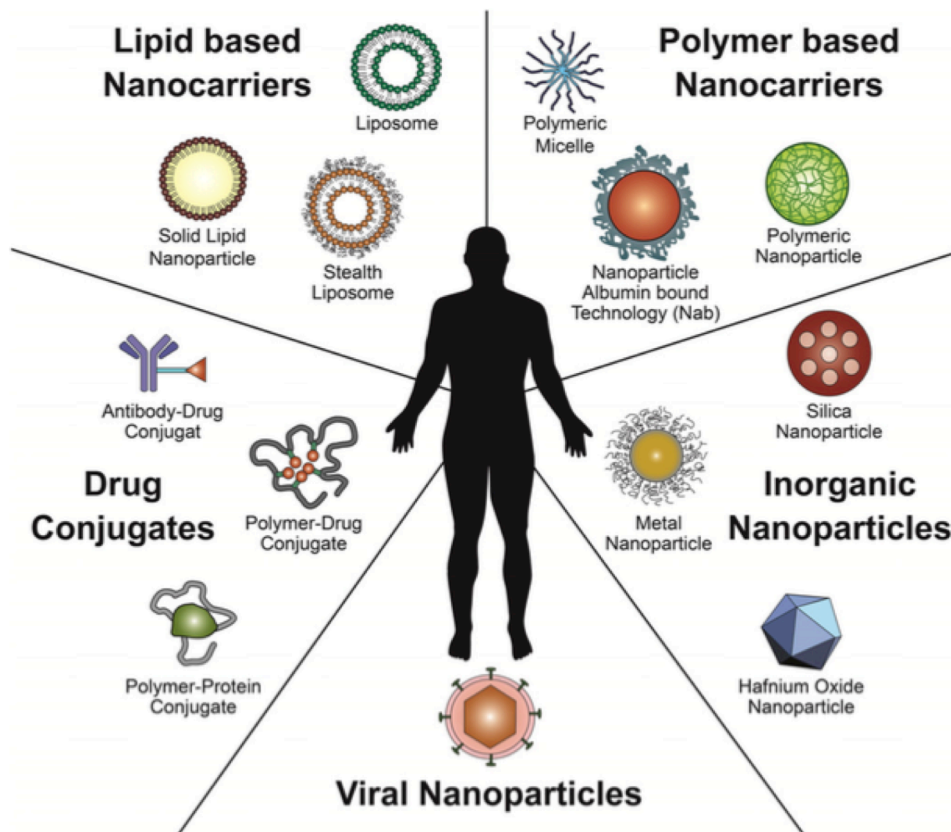
Figure. 4 Schematic illustration of established nanotherapeutic platforms.

Different nanomedicine products such as drug conjugates, lipid-based nanocarriers, polymer-based nanocarriers, inorganic nanoparticles, and viral nanoparticles are used in clinical cancer care. The copyright is owned by the Elsevier, from which permission to reproduce this figure was obtained [2].
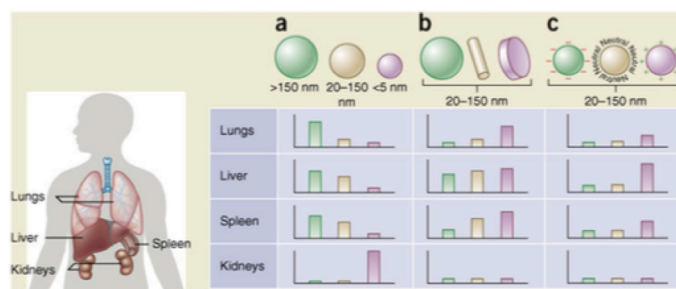
Figure. 5 Nanoparticle size, shape and surface charge dictate biodistribution among the different organs including the lungs, liver, spleen and kidneys. (**a**) Spherical particles, including gold nanoparticles, liposomes and polymeric micelles/nanoparticles can vary in size and display disparate in vivo fates. Large rigid particles with diameters >2,000 nm accumulate readily within the spleen and liver, as well as in the capillaries of the lungs. Nanoparticles in the range of 100–200 nm have been shown to extravasate through vascular fenestrations of tumors (the EPR effect) and escape filtration by liver and spleen. As size increases beyond 150 nm, more and more nanoparticles are entrapped within the liver and spleen. Small-sized nanoparticles (<5 nm) are filtered out by the kidneys. (**b**) Novel 'top-down' and 'bottom up' fabrication techniques have enabled the exploration of different geometries of nanoparticles, including cylindrical and discoidal shapes, which have been shown to exhibit pronounced effects on pharmacokinetics and biodistribution. Different nanoparticle shapes exhibit unique flow characteristics that substantially alter circulating lifetimes, cell membrane interactions and macrophage uptake, which in turn affect biodistribution among the different organs. (**c**) Charge of nanoparticles stemming from distinct surface chemistries influences opsonization, circulation times and interaction with resident macrophages of organs comprising the MPS, with positively charged particles more prone to sequestration by macrophages in the lungs, liver and spleen. Neutral and slightly negatively charged nanoparticles have longer circulation lifetimes and less accumulation in the aforementioned organs of the MPS. In both **b** and **c**, the size of the nanoparticles is assumed to range from 20–150 nm. Individual panels represent in vivo fates of nanoparticles, taking into account singular design parameters of size, shape and surface charge independent of one another, and for this reason, respective scales vary from one panel to the next. It is important to note that in vivo biodistribution will undoubtedly vary based on the interplay of several of the above parameters. The copyright is owned by the Nature Publishing Group, from which permission to reproduce this figure was obtained [6].

I-4 Sakurai's previous technology: ODN/SPG complex

1.1 Schizophyllan (SPG)

Chinese herbal medicine has a long history, probably extending back to about 2500 to 3000 years ago. Over the course of this history, some fungi were recognized as potential medicines to cure gynecological diseases [17]. Modern chemistry subsequently revealed that the active ingredients of such fungi are polysaccharides belonging to the β-1,3-glucan family [18]. Among others, schizophyllan (SPG; see Figure 6 for the chemical structure) [19,20] and lentinan [18] have been commercialized as medicines for uterine cancers in Japan. Immunological studies have shown that these glucans can activate natural immunity by promoting the secretion of interleukins [18]. Toll-like receptors are known to be responsible for the recognition of β-1,3-glucans and to induce the up-regulation of these biological responses. The chemistry of β-1,3-glucans has a relatively long history, whereas the immunological and molecular biological study of β-1,3-glucans has just started, since the finding of Toll-like receptors. Atkins [21] and Sarko [22,23] showed that the simplest β-1,3-glucan, known as curdlan (Figure 5), forms a triple helix in nature. Norisuye et al. [24-26] carefully studied the dilute solution properties of SPG and clarified that it dissolves in water as a triple helix (t-SPG) and in dimethylsulfoxide (DMSO) as a single chain (s-SPG). Furthermore, when water is added to s-SPG/DMSO solution, t-SPG is regenerated from three s-SPG chains via hydrophobic and hydrogen bonding interactions (known as the renaturation process) [27]. Although the renatured product is not exactly the same as the original rod-like molecules, the local structure was proved to restore the triple helix [27,28].
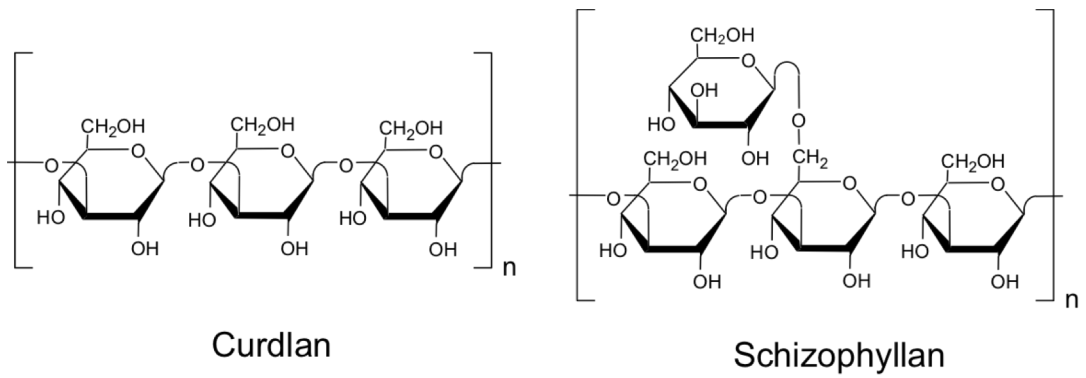
Figure. 6 Chemical strictures of Curdlan and Schizophyllan(SPG).

1.2 ODN/SPG complex

In 2000, Sakurai et al. found that SPG can form a macromolecular complex with several homo-phosphodiester polynucleotides, such as poly(C), poly(A), poly(U), poly(dA), and poly(T), when the polynucleotide is present during the renaturation process of single-chain SPG (s-SPG) [29-33]. The novel features possessed by this complex include: (1) remarkable stability (large binding constant) and water solubility under physiological conditions, (2) the formation of a highly stoichiometric complex, with the stoichiometric number indicating the interaction between two s-SPG units and three base units (i.e., two main chain glucoses vs. one nucleotide) [29], (3) immediate dissociation of the complex followed by hybridization when the s-SPG/DNA complex meets the corresponding complementary sequence [e.g., s-SPG/poly(T) meets poly(dA)], and inhibition (or reduction) of non-specific interactions between bound therapeutic ODNs and serum proteins. They have been exploring this novel polysaccharide/polynucleotide complex and have proposed a new method to deliver DNA by using this complex.

1.3 Spectroscopic changes upon complexation with poly(C) and s-SPG

Figure 7 shows a comparison of the ultraviolet (UV) absorbance and circular dichroism (CD) spectra between poly(C) itself and the complex made from poly(C) and s-SPG (denoted as poly(C)/s-SPG). Here, the M_w (weight-average molecular weight) of s-SPG is 150 kDa and the cytosine base number is about 250. The complexation decreases the absorbance of cytosine at 270 nm by 12% (hypochromic effect), increases the CD intensity of the 275-nm positive band, and creates a new broad band at around 245 nm. Since SPG does not have any functional group to absorb the light within this wavelength range, the hypochromic effect of UV should be ascribed to decreasing distance between the stacked bases in the polynucleotides. Furthermore, the increment

of CD spectral intensity implies that the polynucleotide adopts an ordered helical structure even after complexation, and the content of the helical structure (or the ordering of it) is increased. Consequently, the complexation creates a new ordered helical structure of poly(C). This is in strong contrast to polycation/polynucleotide complexes, in which the CD spectrum is usually considerably suppressed due to random aggregation.

They examined whether the other glucans show similar changes in the UV and CD spectra upon treatment in the same manner as described above. The results shown in Table 2 indicate that complexation is only observed for β-1,3-glucans. Although the data are not shown, no appreciable change was observed in the CD and UV spectra, even when the natural triple helix of SPG was mixed with poly(C). This shows that the renaturation process is indispensable for complexation.
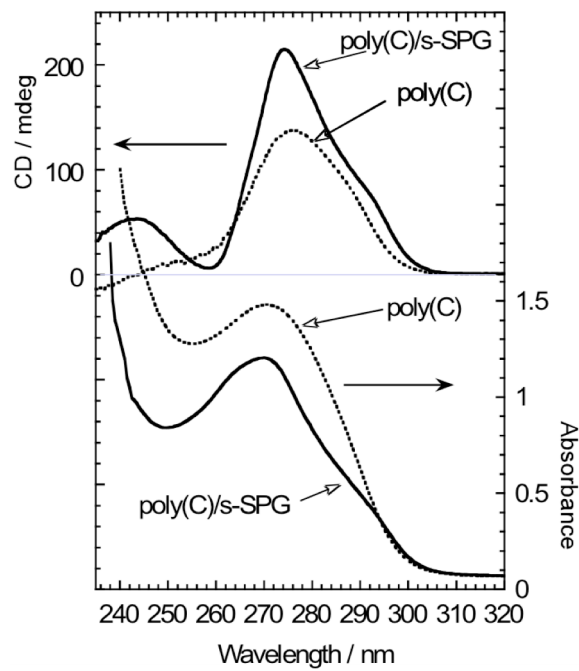
Figure. 7 Comparison of the UV and CD spectra between poly(C) and

poly(C)/s-SPG.

Table 1. Relationship between the capability to form the complex and the glucose linkage of natural glucans. (Permission obtained from Nature Publishing Group)

Name	Units	Linkage	Side chain	
Amylose	α-D-Glucose	1→4	No	No
Carrageenan	β-D-Galactose	Alternating 1→4 and 1→3	Sulfonic groups	No
Cellulose	β-D-Glucose	1→4	No	No
Dextran	α-D-Glucose	1→6	a(1→3) or a(1→4)	No
Pullulan	α-D-Glucose	1→6	No	No
Lentinan	β-D-Glucose	1→3	G G -G-G-G-G-G-	Yes
Curdlan	β-D-Glucose	1→3	-G-G-G-G-G-	Yes
Schizophyllan	β-D-Glucose	1→3	G -G-G-G-	Yes

I-5 Purpose of Thesis and Contents

1.1 The formation of Crosslinked(CL)-ODN through DNA-DNA hybridization

The particle size design for DDS is one of important point. In this research, the particle size was focused based on original ODN/SPG complex. The novel complex was created as a nanogel made from ODN/SPG complexes through DNA–DNA hybridization [crosslinked (CL)-ODN] based on a size-based nanocarrier. In Chapter II describes the formation of crosslinked (CL)-ODN consisting of β-glucan with ODN through DNA hybridization. (Figure 8A)

1.2 CpG-ODN delivery and its immune activity for immune vaccine by the crosslinked(CL)-CpG/SPG complex

CpG-ODN is known as a ligand of Toll-like receptor (TLR) 9 and strongly induces Th1 responses. In Sakurai's previous study, they developed a CpG-ODN delivery system by using CpG/SPG and demonstrated that CpG/SPG induces high T_h1 responses. The CL-ODN include CpG-ODN (denoted CL-CpG) can deliver CpG-ODN to antigen presenting cells. In Chapter III describes cellular uptake of size-controlled CL-CpG and Its enhanced immunostimulation for cancer vaccine and antigen protein model in vitro. (Figure 8B)

1.3 Cytosol delivery by use of TAT-ODN/SPG complex

ODN/SPG complex protects anti-absorption of protein and the ODN is not degraded by enzyme. However the ODN/SPG doesn't have ability of endosome escape. TAT peptide based on lysine rich sequence is well-known improvement target molecule for cellular uptake. For the cytosol delivery of ODN/SPG complex, TAT was conjugated with dA_{40}. The synthesis was based on the crick chemistry. The result, the TAT/ODN/SPG complex was formed. In Chapter IV, the TAT/ODN/SPG complex was characterized

physical and observed distribution in the cell. The antisense (AS)-ODN effect with TAT/AS-ODN/SPG complex was measured in vitro (Figure 8C)

1.4 A two-component micelle with emergent pH responsiveness by mixing dilauroyl phosphocholine and deoxycholic acid and its delivery of proteins into the cytosol

Deoxycholic acid (DA) and its family, generally called bile acids, are known as typical steroid derivatives. The material has long history for medical application and well-known safety. However the material as a DDS doesn't use. Sakaguchi et al. established a new pH-responsive nanoparticle made from dilauroyl phosphocholine (DLPC) and deoxycholic acid. In Chapter , the pH-responsive properties of this system was cleared and to understand its mechanism of action at the molecular level. The resulting, the pH-responsive nanoparticle delivery protein to cytsol.(Figure 8D)

A

Chapter II The formation of Crosslinked(CL)-ODN through DNA-DNA hybridization
Chapter III CpG-ODN delivery and its immune activity for immune vaccine by the crosslinked-CpG/SPG complex
Miyamoto, N., et. al., (2014). Chem. Lett. 43, 991-993
Miyamoto, N. et. al., (2016). ACS Bioconjugate, 28, 565–573
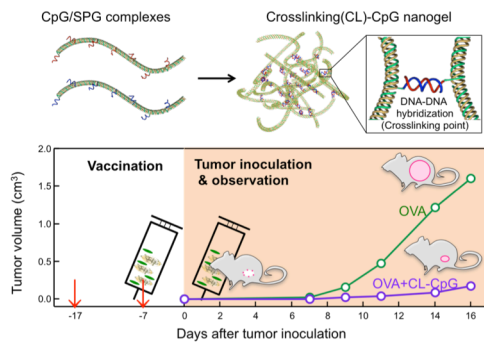
C

Chapter V A two-component micelle with emergent pH responsiveness by mixing dilauroyl phosphocholine and deoxycholic acid and its delivery of proteins into the cytosol
Miyamoto, N. et. al., (2016). Colloids and surfaces B

A Protein delivery to Cytosol with the DLPC/DA
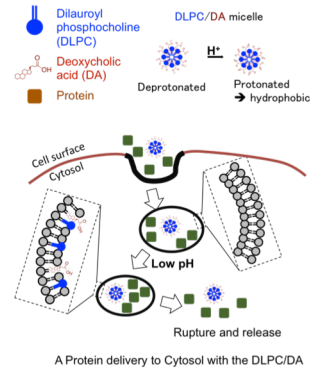
B

Chapter IV Cytosol delivery by use of TAT-ODN/SPG complex

Maegawa, Y. et. al., (2016). Bioorganic & medicinal chemistry letters 26, 1276-1278.
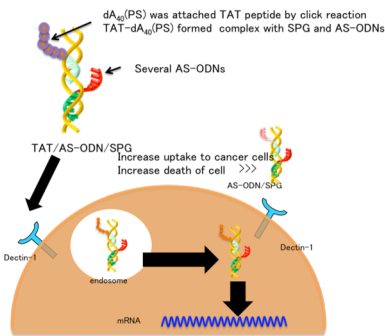
Figure8. The outline of these Chapters

I-5 References

(1)   Melero, I., Gaudernack, G., Gerritsen, W., Huber, C., Parmiani, G., Scholl, S., Thatcher, N., Wagstaff, J., Zielinski, C., and Faulkner, I. (2014) Therapeutic vaccines for cancer: an overview of clinical trials. *Nature reviews Clinical oncology 11*, 509-524.

(2)   Wicki, A., Witzigmann, D., Balasubramanian, V., and Huwyler, J. (2015) Nanomedicine in cancer therapy: challenges, opportunities, and clinical applications. *Journal of Controlled Release 200*, 138-157.

(3)   Stewart, B., and Wild, C. P. (2016) World cancer report 2014. *World*.

(4)   Desmet, C. J., and Ishii, K. J. (2012) Nucleic acid sensing at the interface between innate and adaptive immunity in vaccination. *Nature Reviews Immunology 12*, 479-491.

(5)   van der Burg, S. H., Arens, R., Ossendorp, F., van Hall, T., and Melief, C. J. (2016) Vaccines for established cancer: overcoming the challenges posed by immune evasion. *Nature Reviews Cancer 16*, 219-233.

(6)   Blanco, E., Shen, H., and Ferrari, M. (2015) Principles of nanoparticle design for overcoming biological barriers to drug delivery. *Nature biotechnology 33*, 941-951.

(7)   Schultz, M. (2008) Rudolf Virchow. *Emerging infectious diseases 14*, 1480.

(8)   Grivennikov, S. I., Greten, F. R., and Karin, M. (2010) Immunity, Inflammation, and Cancer. *Cell 140*, 883-899.

(9)   Schreiber, R. D., Old, L. J., and Smyth, M. J. (2011) Cancer immunoediting: integrating immunity's roles in cancer suppression and promotion. *Science 331*,

1565-1570.

(10)   Schlecker, E., Fiegler, N., Arnold, A., Altevogt, P., Rose-John, S., Moldenhauer, G., Sucker, A., Paschen, A., von Strandmann, E. P., and Textor, S. (2014) Metalloprotease-Mediated Tumor Cell Shedding of B7-H6, the Ligand of the Natural Killer Cell–Activating Receptor NKp30. *Cancer research 74*, 3429-3440.

(11)   Cheever, M. A., Allison, J. P., Ferris, A. S., Finn, O. J., Hastings, B. M., Hecht, T. T., Mellman, I., Prindiville, S. A., Viner, J. L., and Weiner, L. M. (2009) The prioritization of cancer antigens: a national cancer institute pilot project for the acceleration of translational research. *Clinical Cancer Research 15*, 5323-5337.

(12)   Rosenberg, S. A., Yang, J. C., and Restifo, N. P. (2004) Cancer immunotherapy: moving beyond current vaccines. *Nature medicine 10*, 909-915.

(13)   Purcell, A. W., McCluskey, J., and Rossjohn, J. (2007) More than one reason to rethink the use of peptides in vaccine design. *Nature reviews Drug discovery 6*, 404-414.

(14)   Janeway, C. A. (1989) in *Cold Spring Harbor symposia on quantitative biology* pp 1-13, Cold Spring Harbor Laboratory Press.

(15)   Reed, S. G., Orr, M. T., and Fox, C. B. (2013) Key roles of adjuvants in modern vaccines. *Nature medicine 19*, 1597-1608.

(16)   Strebhardt, K., and Ullrich, A. (2008) Paul Ehrlich's magic bullet concept: 100 years of progress. *Nature Reviews Cancer 8*, 473-480.

(17)   Hobbs, C. (2000) Medicinal Value of <i>Lentinus edodes</i> (Berk.) Sing. (Agaricomycetideae). A Literature Review.   *2*, 16.

(18)   Chihara, G., Maeda, Y., Hamuro, J., Sasaki, T., and Fukuoka, F. (1969) Inhibition of mouse sarcoma 180 by polysaccharides from Lentinus edodes (Berk.) sing. *Nature 222*, 687-688.

(19)   Tabata, K., Ito, W., Kojima, T., Kawabata, S., and Misaki, A. (1981) Ultrasonic degradation of schizophyllan, an antitumor polysaccharide produced by Schizophyllum commune Fries. *Carbohydrate research 89*, 121-135.

(20)   Suzuki, T., Tsuzuki, A., Ohno, N., Ohshima, Y., Adachi, Y., and Yadomae, T. (2002) Synergistic action of beta-glucan and platelets on interleukin-8 production by human peripheral blood leukocytes. *Biological & pharmaceutical bulletin 25*, 140-144.

(21)   Atkins, E. D. T., and Parker, K. D. (1968) Cyclic Triad of Hydrogen Bonds in a Helical Polymer. *Nature 220*, 784-785.

(22)   Deslandes, Y., Marchessault, R. H., and Sarko, A. (1980) Triple-Helical Structure of(1→3)-β-D-Glucan. *Macromolecules 13*, 1466-1471.

(23)   Bluhm, T. L., and Sarko, A. (1977) The triple helical structure of lentinan, a linear β-(1 → 3)-D-glucan. *Canadian Journal of Chemistry 55*, 293-299.

(24)   Yanaki, T., Norisuye, T., and Fujita, H. (1980) Triple Helix of Schizophyllum commune Polysaccharide in Dilute Solution. 3. Hydrodynamic Properties in Water. *Macromolecules 13*, 1462-1466.

(25)   Norisuye, T., Yanaki, T., and Fujita, H. (1980) Triple helix of a schizophyllum commune polysaccharide in aqueous solution. *Journal of Polymer Science: Polymer Physics Edition 18*, 547-558.

(26)   Kashiwagi, Y., Norisuye, T., and Fujita, H. (1981) Triple helix of

Schizophyllum commune polysaccharide in dilute solution. 4. Light scattering and viscosity in dilute aqueous sodium hydroxide. *Macromolecules 14*, 1220-1225.

(27)   Sato, T., Norisuye, T., and Fujita, H. (1983) Triple helix of Schizophyllum commune polysaccharide in dilute solution. 5. Light scattering and refractometry in mixtures of water and dimethyl sulfoxide. *Macromolecules 16*, 185-189.

(28)   Stokke, B. T., Elgsaeter, A., Brant, D. A., Kuge, T., and Kitamura, S. (1993) Macromolecular cyclization of $(1 \rightarrow 6)$-branched-$(1 \rightarrow 3)$-β-D-glucans observed after denaturation–renaturation of the triple-helical structure. *Biopolymers 33*, 193-198.

(29)   Koumoto, K., Kimura, T., Kobayashi, H., Sakurai, K., and Shinkai, S. (2001) Chemical Modification of Curdlan to Induce an Interaction with Poly(C). *Chemistry Letters 30*, 908-909.

(30)   Miyoshi, K., Uezu, K., Sakurai, K., and Shinkai, S. (2004) Proposal of a New Hydrogen-Bonding Form to Maintain Curdlan Triple Helix. *Chemistry & Biodiversity 1*, 916-924.

(31)   Sakurai, K., and Shinkai, S. (2000) Molecular Recognition of Adenine, Cytosine, and Uracil in a Single-Stranded RNA by a Natural Polysaccharide: Schizophyllan. *Journal of the American Chemical Society 122*, 4520-4521.

(32)   Sakurai, K., Mizu, M., and Shinkai, S. (2001) Polysaccharide−Polynucleotide Complexes. 2. Complementary Polynucleotide Mimic Behavior of the Natural Polysaccharide Schizophyllan in the Macromolecular Complex with Single-Stranded RNA and DNA. *Biomacromolecules 2*, 641-650.

(33) Koumoto, K., Kimura, T., Mizu, M., Kunitake, T., Sakurai, K., and Shinkai, S. (2002) Polysaccharide-polynucleotide complexes. Part 12. Enhanced affinity for various polynucleotide chains by site-specific chemical modification of schizophyllan. *Journal of the Chemical Society, Perkin Transactions 1*, 2477-2484.

Chapter II

Crosslinked oligonucleotides(ODN)/β-1,3-Glucan Nanoparticle through DNA-DNA Hybridization.

II.1 Introduction

The nanoparticle size depends on cells and endocytosis pathways, its range is normally a few hundred nm.[1] In a design of nanoparticle for drug delivery, the size is one of important point. Sakurai et al. studies,[2,3] there is a particular range in nanoparticle size suitable for cellular uptake.

We have studied a polysaccharide schizophyllan (SPG), a member of β-glucans, as a delivery carrier of ODN since SPG can make a complex with specific homonucleotides such as poly(C) or poly(dA) via a combination of hydrogen bonding and hydrophobic interactions.[4-6] As presented in Figure 1, two SPG chains and one polynucleotide chain form a triple helix through the binding between two main chain glucoses and one base. The complex can be recognized by Dectin-1 on APCs and then incorporated into the cells.[2,3] Dectin-1 is a major receptor involved in the recognition of β-glucans on APCs, including macrophages dendritic cells, monocytes, neutrophils, and B cells. [7,8] Thus, it is expected that β-glucans can specifically deliver the bound ODN to APCs. We have reported that antisense ODN or short interference RNA complexed with SPG shows efficient gene silencing in animal models of fulminant hepatitis[3,9] and bowl disease.[10] We also have prepared the complex made from CpG-ODN, which is adjuvant, and SPG (CpG-ODN/SPG) and attained the induction of robust immune response in vitro and in vivo.[2,11]

Compared to these sizes, the present ODN/SPG is relatively small when we used SPG with a molecular weight of 150 K (ca., 10-20 nm in diameter). Therefore, the preparation of larger particles with ODN/SPG would enhance performance or add further functionality to the present system.

II.2 Experimental

2.1 Nanoparticle Preparation.

SPG was dissolved in 0.25 N NaOHaq (1 N NaOH; Waco Inc., Osaka, Japan) for two days to dissociate the triple helix into single chains. Appropriate amounts of SPG solution, ODN in water, and phosphate-buffered solution (330 mM NaH_2PO_4, pH = 4.7) were mixed together. Then, this mixture (0.1 μM ODN, pH = 7.4) was stored at 4 °C overnight. The molar ratio of [SPG]/[ODN] was set at 0.27, where seven ODN units are contained in one complex on average. In the same manner, we prepared cODN/SPG. After complexation, ODN/SPG was mixed with cODN/SPG at different mixing ratios and incubated at room temperature overnight. The mixing molar ratio is denoted as CL-ODN (1:X), where X is the molar ratio of cODN/SPG to 1 molar ODN/SPG. We only used CL-ODN (1:1) for in vivo assays and the term CL-ODN refers to this equimolar mixture unless otherwise noted.

2.2 Gel electrophoresis

Nanoparticle was analyzed with 1% agarose gel electrophoresis at 4 °C. After the electrophoresis, ODNs were stained with SYBR Gold (Invitrogen, Carlsbad, CA).

2.3 Physicochemical characterization

Dynamic light scattering (DLS) at a fixed angle of 14–163° was measured with a Malvern Zetasizer Nano (Malvern Instruments, Malvern, UK) at room temperature. The obtained correlation function was converted to the size distribution. A level of solvent viscosity of 0.142 ml/g was used. Based on the obtained distribution, the number-averaged hydrodynamic radius (R_h) was determined. The concentration of the samples was approximately 2.6 mg/ml. Synchrotron small-angle X-ray scattering (SAXS) was measured for ODN/SPG and CL-ODN at the beam-line BL40B2 at

SPring-8, with a 2.0-m camera and an X-ray wavelength of 0.1 nm. The experimental details are reported elsewhere.[12] The weight-averaged molecular weight (M_w) was determined using multi-angle light scattering (MALS) coupled with gel permeation chromatography (GPC).[12] The ratio of double-stranded ODN to single strands was determined using the Quant-iT dsDNA BR Assay Kit (Thermo Fisher Scientific, Hudson, NH, USA).

II.3 Results and Discussions

Creation and physiochemical characterization of CL-ODN nanogel

One way to make a large particle is to use ODN portions as a crosslinking point. We mixed complementary ODN (cODN)- dA_{40}/SPG and ODN-dA_{40}/SPG at the same molar ratio and examined this mixture (denoted cODN-dA_{40}/SPG + ODN-dA_{40}/ SPG) with gel electrophoresis. Here, ODN-dA_{40} and cODN-dA_{40} sequences are ATCGACTCTCGAGCGTTCTC-dA_{40} and GAGAACGCTCGAGAGTCGAT-dA_{40}, respectively; dA_{40} is necessary for binding to SPG.

Figure 2A compares the 1% agarose gel electrophoresis migration patterns, where ODN-dA_{40} and cODN-dA_{40} were stained with SYBR Gold. The cODN-dA_{40}/SPG and ODN-dA_{40}/SPG showed smeary fluorescence bands at the larger molecular weight side than the original ODN-dA_{40} and cODN-dA_{40} did. No migration was observed for the ODN-dA_{40}/ SPG + ODN-dA40/SPG, their fluorescence was retained in the wells, indicating that its molecular size was too large to move through the gel. Based on previous studies,[2,3] we can presume that the ODN or cODN portions in the complex are not involved in the complexation with SPG and exist as a single strand, as presented in Figure 1A. Therefore, after we mixed cODN-dA_{40}/ SPG and ODN-dA_{40}/SPG, some of the ODN portions hybridize with the cODN portion and this hybridization should play the role of crosslinking points, resulting in larger particles than the original ones, as illustrated in Figure 1B. Hereinafter, we denote this component as crosslinked ODN-dA_{40}/SPG nanoparticle. When ODN-dA_{40}/SPG was mixed with non-cODN-dA_{40}/SPG (i.e., scrambled sequence for ODN), the fluorescence was observed at the same position as with ODN-dA_{40}/SPG. Another important conclusion is that there was no applicable amount of ODN-dA_{40}/SPG and cODN-dA_{40}/SPG fluorescence observed after mixing, indicating that the major component of

40

cODN-dA$_{40}$/SPG + ODN-dA$_{40}$/SPG is the nanoparticle.

Figure 2B shows a comparison of the size distribution between ODN-dA$_{40}$/SPG and CL-ODN, obtained by DLS. Mixing ODN/SPG and cODN/SPG together was shown to increase the particle size more than ten times from R_h = 10.1 nm to R_h = 150 nm. This indicates that several crosslinks were formed owing to hybridization between ODN and cODN sequences in CL-ODN. The increased size as well as molecular weight was confirmed by MALS (Figure 2C), in which the main peak was found at an elution time of 20 min and M_w was determined by extrapolating the zero scattering angle using Berry's plot. The values of M_w at the peak top were 5×10^5 g mol^{-1} and 2×10^7 g mol^{-1} for ODN/SPG and CL-ODN, respectively. Owing to a low signal intensity, the radius of gyration could not be determined accurately. Figure 2D plots R_h against the composition of the mixture. As expected, a ratio of ODN/SPG to cODN/SPG of 1:1 gave the highest R_h value. It is interesting that R_h increased exponentially as an equimolar composition was approached. Two conclusions can be drawn from this: First, the exponential increase is consistent with normal gelation theory or behavior, in which the molecular weight increases infinitely at the gelation point.[13] Second, the ODN and cODN portions hanging out from SPG play roles in crosslinking the complex. The size or molecular weight at a mixing ratio of 1:1 remains finite because we carried out the mixing at a relatively low concentration. Therefore, gelation was confined to a certain spatial limit. In this sense, we can regard CL-ODN(1:1) as a nanogel particle similar to cholesterol/pullulan nanogels.[14]

Our previous study[12] showed that ODN/SPG complex (ODN/SPG) adopts the form of a semiflexible rod-like chain without branching, similar to the original triple helix of SPG. These two forms differ with regard to their flexibility: the complex is more flexible than

41

the triple helix of SPG, in terms of the persistence length: 200 nm for the SPG triple helix and 60 nm for the complex. Figure 3 double-logarithmically plots the SAXS intensity [I (q)] against the magnitude of the scattering vector (q) for renatured SPG, ODN/SPG, and CL-ODN. For all samples, intermediate q (0.1 nm^{-1}<q<~0.7 nm^{-1}, corresponding to 60–10 nm in real space) gives a scaling factor of α=-1 when we express q I (q) ∝q^{α}. This means that the local conformation for CL-ODN shows a rod-like nature similar to the complex and SPG. Therefore, it can be concluded that the gelation with ODN/cODN hybridization does not interfere with the rod-like nature of the complex. In the low-q range (q<~0.1 nm^{-1}), α becomes -2 for CL-ODN, while the others showed no change. This difference is due to the presence of a gel network in CL-ODN and the network size can be roughly estimated to be 60 nm. The inset of Figure 3 shows the cross-sectional Guinier plot for the high-q range (i.e., ln q I(q) vs. q^2). From the slope, the cross-sectional radius of gyrations for all samples can be determined (the determined values are indicated in the inset). CL-ODN shows a slightly smaller cross-sectional size. This may be due to averaging of both the thick complex (~0.77 nm in diameter) and the thin double-stranded DNA (~0.72 nm).

The double-stranded ratio was determined to be almost 100% with the BR assay, which reflects an absence of free ODN or cODN portions hanging out from the complex. This is consistent with the gelation behavior shown in Figure2D. Combining the above findings, we can depict the structure of CL-ODN as follows (also shown in Figure 1C). After mixing semi-flexible ODN/SPG and cODN/SPG, the free ODN and cODN portions form a DNA double helix at almost 100% yield; this double-stranded DNA plays a role in the crosslinking that results in gelation. The nanogel particle size is approximately 150 nm and the overall molecular weight is increased by 10 times. Based on this molecular weight, the number of crosslinking DNA can be estimated to be 35

per CL-ODN. Intermediate SAXS shows that the 60–10 nm local structure of CL-ODN is identical to that of ODN/SPG. This is an important conclusion because most molecular pattern recognition receptors recognize structures of this size. The unchanged local conformation was also confirmed by circular dichroism (see Figure S1).

II.4 Conclusions

In conclusion, we prepared a crosslinked nanoparticle consisting of ODN-dA$_{40}$/SPG and cODN-dA$_{40}$/SPG complexes through DNA-DNA hybridization. This nanoparticle was much larger and controlled the particle size by mixing complex ratio showed. The present study suggests that the crosslink complex can be used as a potent gene delivery to expression Dectin-1 cell.

II.5 Figures
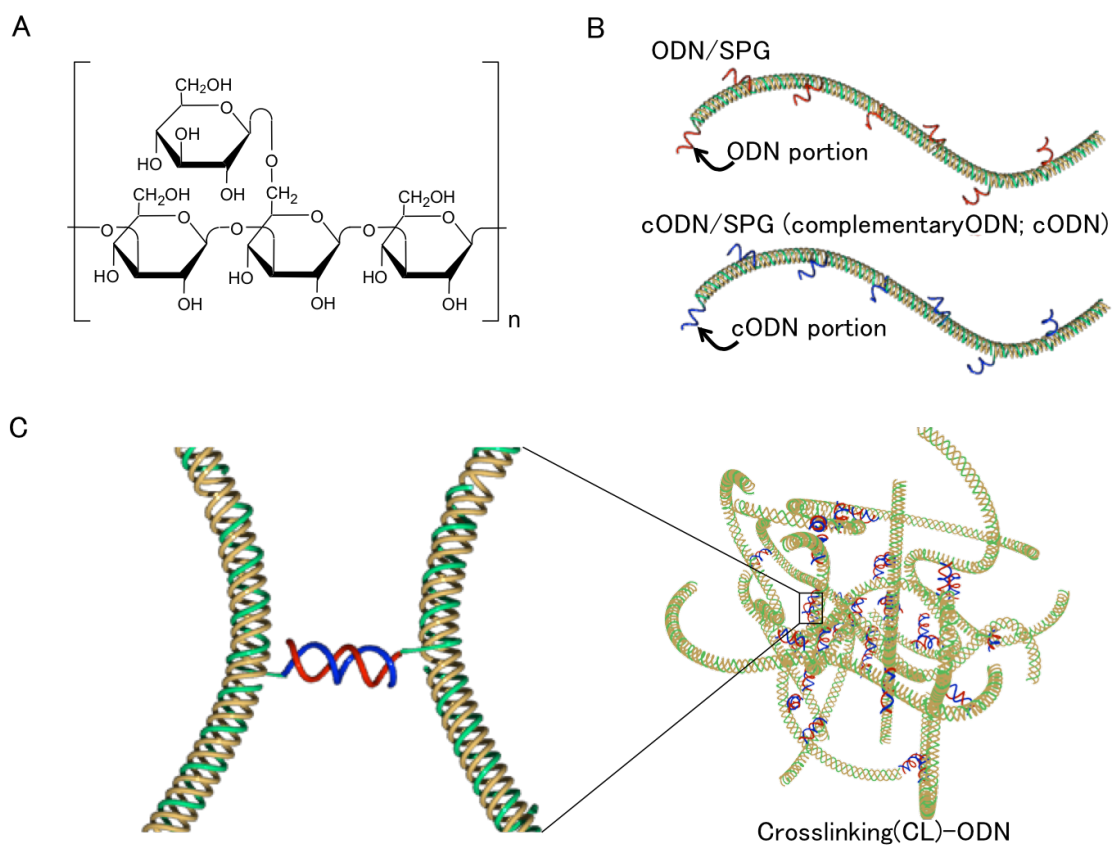
Figure 1. Schematic illustration of CL-ODN nanogel, with the chemical structure of SPG shown in A. The ODN/SPG and cODN/SPG complexes have a single chain of ODN or cODN hanging out from the dA_{40}/SPG complex. (B) After mixing, hybridization between ODN and cODN leads to the formation of a nanogel. (C) In this nanogel, the characteristic semiflexible rod-like structure is maintained, which can be recognized by Dectin-1 and other β-1, 3-glucan receptors on APCs. The network size is determined to be 60 nm using small- angle X-ray scattering.
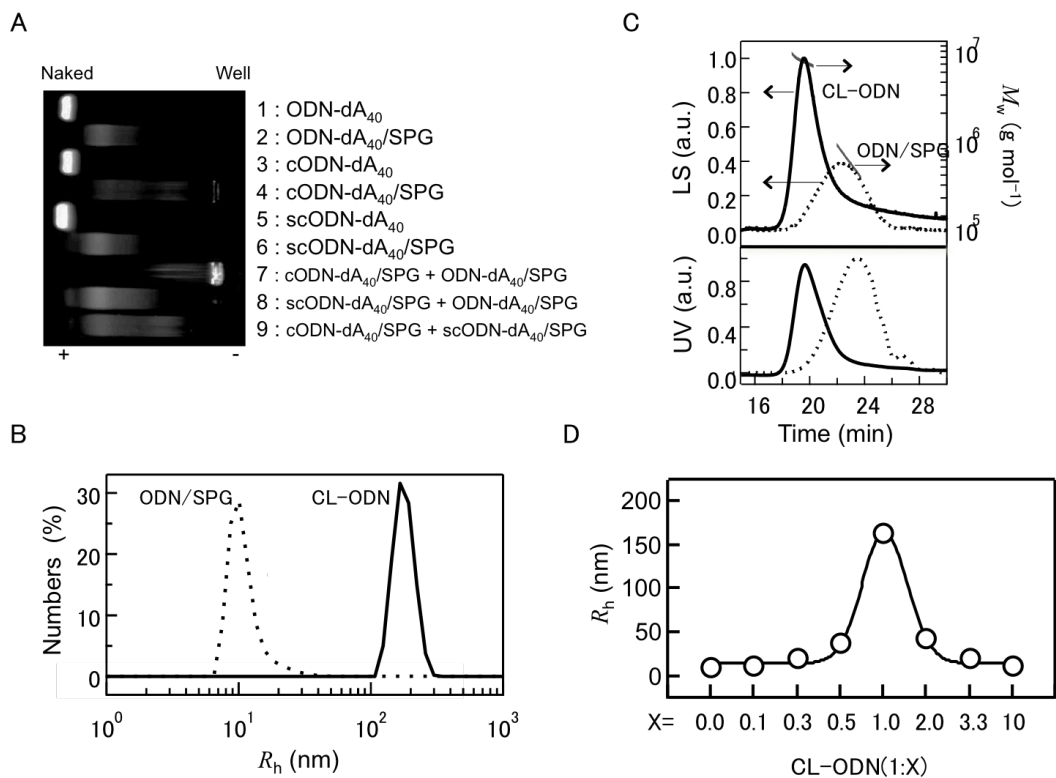
Figure 2. Increased molar mass due to crosslinking between ODN-dA$_{40}$/SPG and cODN-dA$_{40}$/SPG, observed with (A) 1wt % agarose gel electrophoresis. Particle size evaluation by DLS (B, D) and molecular weight determination by GPC coupled with MALS (C). The ODN/SPG and cODN/SPG mixing composition dependence of Rh, showing that gelation occurred at a ratio of 1:1.
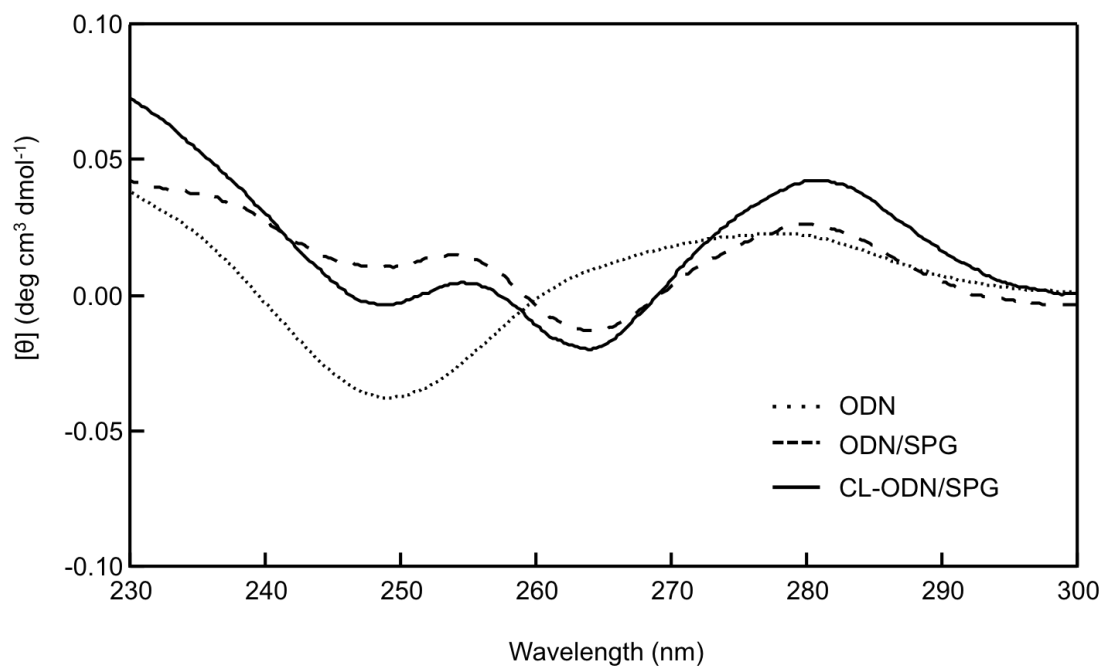
Supporting Figure 1. The structural changes of ODN after complexation with SPG and nanogel formation. The circular dichroism spectra at 240–320 nm for ODN (red short dotted line), ODN/SPG (black long dotted line), and CL-ODN (black solid line) were measured at room temperature.

II.6 References

(1)   Gratton, S. E., Ropp, P. A., Pohlhaus, P. D., Luft, J. C., Madden, V. J., Napier, M. E., and DeSimone, J. M. (2008) The effect of particle design on cellular internalization pathways. *Proc Natl Acad Sci U S A 105*, 11613-11618.

(2)   Minari, J., Mochizuki, S., Matsuzaki, T., Adachi, Y., Ohno, N., and Sakurai, K. (2011) Enhanced cytokine secretion from primary macrophages due to Dectin-1 mediated uptake of CpG DNA/beta-1,3-glucan complex. *Bioconjug Chem 22*, 9-15.

(3)   Mochizuki, S., and Sakurai, K. (2011) Dectin-1 targeting delivery of TNF-alpha antisense ODNs complexed with beta-1,3-glucan protects mice from LPS-induced hepatitis. *J Control Release 151*, 155-161.

(4)   Sakurai, K., and Shinkai, S. (2000) Molecular Recognition of Adenine, Cytosine, and Uracil in a Single-Stranded RNA by a Natural Polysaccharide: Schizophyllan. *J. Am. Chem. Soc. 122*, 4520-4521.

(5)   Sakurai, K., Mizu, M., and Shinkai, S. (2001) Polysaccharide--polynucleotide complexes. 2. Complementary polynucleotide mimic behavior of the natural polysaccharide schizophyllan in the macromolecular complex with single-stranded RNA and DNA. *Biomacromolecules 2*, 641-650.

(6)   Mizu, M., Kimura, T., Koumoto, K., Sakurai, K., and Shinkai, S. (2001) Thermally induced conformational transition of polydeoxyadenosine in the complex with schizophyllan and the base-length dependence of its stability. *Chem. Commun.*, 429-430.

(7)   Brown, G. D., and Gordon, S. (2001) Immune recognition. A new receptor for

beta-glucans. *Nature 413*, 36-37.

(8) Brown, G. D., Taylor, P. R., Reid, D. M., Willment, J. A., Williams, D. L., Martinez-Pomares, L., Wong, S. Y., and Gordon, S. (2002) Dectin-1 is a major beta-glucan receptor on macrophages. *J Exp Med 196*, 407-412.

(9) Mochizuki, S., Morishita, H., and Sakurai, K. (2013) Macrophage specific delivery of TNF-alpha siRNA complexed with beta-1,3-glucan inhibits LPS-induced cytokine production in a murine acute hepatitis model. *Bioorg Med Chem 21*, 2535-2542.

(10) Takedatsu, H., Mitsuyama, K., Mochizuki, S., Kobayashi, T., Sakurai, K., Takeda, H., Fujiyama, Y., Koyama, Y., Nishihira, J., and Sata, M. (2012) A new therapeutic approach using a schizophyllan-based drug delivery system for inflammatory bowel disease. *Mol Ther 20*, 1234-1241.

(11) Kobiyama, K., Aoshi, T., Narita, H., Kuroda, E., Hayashi, M., Tetsutani, K., Koyama, S., Mochizuki, S., Sakurai, K., Katakai, Y., et al. (2014) Nonagonistic Dectin-1 ligand transforms CpG into a multitask nanoparticulate TLR9 agonist. *Proc Natl Acad Sci U S A*.

(12) Sanada, Y., Matsuzaki, T., Mochizuki, S., Okobira, T., Uezu, K., and Sakurai, K. (2012) beta-1,3-D-glucan schizophyllan/poly(dA) triple-helical complex in dilute solution. *J Phys Chem B 116*, 87-94.

(13) Barnes, H. A., Hutton, J. F., and Walters, K. (1989) *An introduction to rheology*, Vol. 3, Elsevier.

(14) Akiyoshi, K., Sasaki, Y., and Sunamoto, J. (1999) Molecular chaperone-like activity of hydrogel nanoparticles of hydrophobized pullulan: thermal

stabilization with refolding of carbonic anhydrase B. *Bioconjugate Chemistry 10*, 321-324.

Chapter III

Adjuvant activity enhanced by crosslinked CpG-oligonucleotides in beta-glucan nanogel and its anti-tumor effect

III.1 Introduction

Several remarkable breakthroughs have been made in cancer immunotherapy in the last few years.[1,2] Among them, promising levels of therapeutic efficacy have been reported in solid tumors by inhibiting T-cell checkpoint molecules such as PD-1 using monoclonal antibodies.[3] Another breakthrough has been achieved by ex vivo engineering of T-cell therapy.[4] Compared with these two approaches, cancer vaccines have failed to show convincing results regarding their efficacy in humans,[5] although they have a long history in tumor immunotherapy since the mid-1990s.[5,6] Recent immunological studies revealed that there are several factors behind this lack of success. According to the recent reviews,[7] these factors are (1) poor antigenicity of tumor antigen, (2) heterogeneous expression of tumor antigen, (3) a lack of an optimal vaccine administration schedule and route, (4) how to choose a suitable adjuvant, and (5) an immunosuppressive status at both local and systemic levels. To improve the effectiveness of cancer vaccines, we need to develop a new vaccine system by taking these issues into account.[8,9]

When an antigen is administered in the process of cancer vaccination, it is first taken up by phagocytosis of antigen-presenting cells (APCs) such as dendritic cells and macrophages. After fragmentation and modification, certain small antigen peptides are presented to CD8+ T cells and CD4+ T cells via major histocompatibility complex (MHC) molecules on the surface of APCs.[10,11] The antigen/MHC complex is recognized by T-cell receptors of these two T cells and they eventually mature. The mature CD8+ T cells are essential for eradication of the tumor cells and are called cytotoxic T lymphocyte (CTLs). However, the addition of an antigen alone does not induce a sufficient immune response to attack cancer cells. Similar to other vaccines, there is a need to add an adjuvant that can modify the immune response by helping immature to

lead a mature. Ligands or agonists that can be recognized by Toll-like receptors (TLRs) 3, 7, and 9 can be potent adjuvants.[12-14] Among them, CpG oligonucleotides (CpG-ODNs) containing the immunostimulatory CpG motif are an excellent adjuvant and can activate APCs through binding to TLR9.[15,16]

The outcome of CpG-ODN depends on its sequence and backbone.[15,17,18] D-type CpG-ODNs (or CpG-A) contain a palindromic CpG sequence with phosphodiester (PO) backbones connecting with a poly(G)-tail with phosphorothioate (PS) backbones. CpG-ODNs are known to lead to the production of large amounts of IFN-α.[19] Their biological outcome may be related to the tendency for the D-type to form large aggregates due to G-quartet-related intermolecular interactions, which may hamper clinical application owing to the side effect caused by its aggregation. Its aggregated structures are supposed to lead to high production of IFN-α.[20] However, Aoshi et al.22 recently found that non-aggregated D-type CpG-ODNs also led to an immune response similar to that with aggregated ones. Therefore, we suppose that the molecular and biological mechanisms of the response to D-type DNAs have not been established yet. It is still the case that their aggregation makes clinical trials difficult, unless the size and time-course stability are well controlled.[21,22] K-type CpG-ODNs (or CpG-B) with PS contain multiple non-palindromic sequences and induce interleukin-6 (IL-6) and the maturation of plasmacytoid dendritic cells.[15,23,24] K-type CpG-ODNs are soluble in aqueous solution, which does not impede clinical trials, and activate B-cells to produce IL-6, but does not produce a large amount of IFN-α. These CpG-ODNs can be an excellent candidate for an adjuvant for vaccination. However, they have several drawbacks that need to be overcome. One of the major problems is that CpG-ODNs are easily degraded by nucleases and excreted into the urine before being taken up by APCs. Phosphorothioate or other artificially modified nucleotide analogues may prevent such

degradation, but the chemical modification may cause side effects.[25] Furthermore, a suitable delivery vehicle to transport the CpG-ODNs to APCs is needed to improve immunostimulatory specificity and immunotherapeutic efficiency.

Recently, we have demonstrated that CpG-ODNs can be specifically delivered to APCs and stimulate human peripheral blood mononuclear cells to produce large amounts of both type I and II IFN, when CpG-ODNs are complexed with a beta-glucan SPG.[26-29] Here SPG is an abbreviation of schizophyllan, which is a member of the beta-glucans and comprises a main (1→3)-beta-D-glucan chain and a (1→6)-beta-D-glycosyl side chain that links to the main chain at every third glucose residue (Figure 1A). SPG forms a stoichiometric complex with specific homo-nucleotides such as poly(C) or poly(dA).[30] Furthermore, SPG and its complex with ODN can be specifically recognized and then taken up by certain Immunocytes. The great advantage of the CpG-ODN/SPG complex (CpG/SPG) is that, when K-type CpG-ODN was administered as an SPG complex, it led to the production of a large amount of IFN-α and CTL induction at the same time. The CpG-ODN is not necessary to bind to antigens. The drastic antigen-specific response can be obtained only upon co-administration of protein antigens.[28,29] These novel and quite effective adjuvant properties are considered to be attributable to the nano-particle nature of the CpG/SPG complex.[28] Therefore, in this study, we increased the particle size of the complex and examined its immune response and adjuvant effect as a cancer vaccine.

APCs express several receptors to bind beta-glucans including Dectin-1, which explains why we can specifically deliver ODNs/SPG to them. According to recent studies, particle size, morphology, and surface characteristics are important factors to promote cellular uptake.[31-33] This is especially true for phagocytic APCs. Bachmann et al. demonstrated that nanoparticles of 20–200 nm in size are likely to accumulate in

dendritic cells and macrophages residing in draining lymph nodes.[34] In a Chapter 2 , ODN/SPG was determined to be approximately 10–20 nm in diameter,[27] and this smaller size seemed to be less uptaking by APCs. We can thus expect that larger CL-ODN particles would enhance this uptake. In the chapter II,[27] we reported a new concept of forming a larger ODN/SPG nanogel particle (denoted CL-ODN, where CL stands for crosslink) than normal complexes by using crosslinks between ODN/SPG and complementary ODN (cODN)/SPG complexes (cODN/SPG) through DNA-DNA hybridization. In the present study, which continues on from this previous work, we report that the including CpG-ODN of CL-CpG was examined the adjuvant efficiency of the cancer vaccine in vivo.

III.2 Experimental

2.1 Materials

SPG ($M\_w = 1.5 \times 10^5$ as a single chain) was kindly provided by Mitsui Sugar Co., Ltd. (Tokyo, Japan). All DNAs were synthesized by Gene Design Inc. (Osaka, Japan) and purified using high-performance liquid chromatography. In this study, we used a PS instead of a PO for dA since PS-dA forms a stable complex with SPG compared with PO-dA.[35] The sequences of CpG and cCpG are ATCGACTCTCGAGCGTTCTC-dA$_{40}$ and GAGAACGCTCGAGAGTCGAT-dA$_{40}$. EndoFitTM ovalbumin (OVA) was purchased from InvivoGen (San Diego, CA, USA). As an antigenic peptide, an OVA peptide (SIINFEKL, amino acids 257–264 from OVA; OVA257–264) was synthesized by Gene Design Co., Ltd. IL-6 and IFN-γ ELISA kits were purchased from eBioscience, Inc. (San Diego, CA, USA).

2.2 CL-CpG/SPG preparation

SPG was dissolved in 0.25 N NaOHaq (1 N NaOH; Waco Inc., Osaka, Japan) for two

days to dissociate the triple helix into single chains. Appropriate amounts of SPG solution, CpG in water, and phosphate-buffered solution (330 mM NaH_2PO_4, pH = 4.7) were mixed together. Then, this mixture (0.1 μM CpG, pH = 7.4) was stored at 4 °C overnight. The molar ratio of [SPG]/[CpG] was set at 0.27, where seven CpG units are contained in one complex on average.[27] In the same manner, we prepared cCpG/SPG. After complexation, CpG/SPG was mixed with cCpG/SPG at equal molar ratios and incubated at room temperature overnight.

2.3 Cells lines

RAW 264 (a murine macrophage cell line from blood) and E.G7-OVA cells (OVA-transfected EL4 thymoma cells) were purchased from American Type Culture Collection (Manassas, VA, USA) and cultured in RPMI 1640 medium (Waco Inc., Osaka, Japan) at 37 °C in 5% CO2.

2.4 Uptake of fluorescein isothiocyanate (FITC)-labeled SPG into immune cells

FITC-labeled SPG (denoted f-SPG) was prepared by a previously reported method and, on average, FITC was attached to one of every 13 glucoses on the main chain.[36,37] We confirmed that attachment of FITC at this low level did not interfere with any characteristics of the complex. An f-SPG solution of 7.5 μg/mL was added to 4 × 104 cells/96-well plate. After the indicated times, cells were washed twice with PBS, stained with 4′, 6-diamidino-2-phenylindole, and the cellular image was observed with a BZ-9000 fluorescence microscope (Keyence Co., Osaka, Japan). For the measurement of fluorescence intensities, the homogenates were prepared with lysis buffer. The fluorescence intensities and protein concentrations were measured with a Wallac 1420 (PerkinElmer, Wellesley, MA, USA) and a Protein Quantification Kit (Dojindo, Kumamoto, Japan), respectively.

2.5 Mice

All mouse experiments were performed in accordance with the guidelines of the Animal Care and Use Committee of the University of Kitakyushu. Seven-week-old male C57BL/6J mice were purchased from Japan SLC, Inc. (Shizuoka, Japan).

2.6 Cytokine secretion assay

Mouse splenocytes were seeded at 1.0×10^6 cells/96-well plate and supplemented with the indicated adjuvants at 200 nM. After 24 h, IL-6 concentrations in the supernatants were measured with a mouse IL-6 ELISA kit.

2.7 Formation of OVA-specific CD8+ cells

Mice were intradermally immunized with OVA (30 μg) combined with CpG, CpG/SPG, or CL-CpG (CpG; 15 μg for all experiments and the DNA dose was fixed at the same amount for the naked and complex administration) at day 0 and day 10. After the collection of mouse splenocytes at day 17, the cells were stimulated with OVA257–264 at 10 μg/ml for 24 h. The supernatants were subjected to ELISA to detect mouse IFN-γ. For the quantitative determination of OVA-specific CD8+ cells, splenocytes were stained with H-2Kb OVA tetramer (MBL Co., Ltd., Nagoya, Japan) and anti-CD8 antibody (BD Pharmingen, San Diego, CA, USA). The population of OVA tetramer+ CD8+ cells was determined with an EPICS® XL flow cytometer (Beckman Coulter, Fullerton, CA, USA).

2.8 Formation of OVA-specific CD8+ cells Tumor growth assay

Mice were pre-immunized with a mixture of OVA and naked CpG, CpG/SPG, or CL-CpG on days −17 and −7 before inoculation with 1.0×10^6 E.G7-OVA cells in the left flank on day 0. The tumor size was monitored by measuring two axes of the tumor

using digital calipers every two to three days. The tumor volume was calculated as follows: "minor axis^2 × major axis × 0.5". Once the tumors had reached 2.5 cm3 in volume, the mice were sacrificed by CO_2 inhalation.

III.3 Results and Discussions

Cellular uptake of CL-CpG

Figure 1A shows the time course of fluoresense microscopic imaging of the RAW 264 cells upon the addition of CL-CpG containing f-SPG [denoted CL-CpG(f)] or CpG/f-SPG. The green fluorescence color originating from FITC became detectable after 4 h, increased its intensity with the passing of time, and reached a maximum after 8 h. At this stage, CL-CpG(f) was uniformly distributed in all of the cells. Figure 1B plots the fluorescence intensity against time, showing that CL-CpG(f) exhibited almost ten times greater intensity than f-SPG and CpG/f-SPG after 24 h. These results indicate that there is a preference for CL-CpG(f) uptake rather than CpG/f-SPG uptake. It is well known that APCs express various receptors including Dectin-1 that can specifically bind to beta-1, 3-glucans,[38,39] and ODN/SPG complex is also recognized by Dectin-1 with the same extent with SPG.[26,40] Therefore, the increased uptake of CL-CpG can be ascribed to increased interaction between beta-1, 3-glucan binding receptors and CL-CpG. In this context, the main cause of this increase is of interest. Figure 1C shows a comparison of the fluorescence images after 4 h for different mixing ratios. This indicates that the cellular uptake peaks at a mixing ratio of 1:1. The structural analysis showed that mixing CpG/SPG and cCpG/SPG does not change the local conformation from the range of 10–60 nm, which is a size range normally recognized by pattern recognition receptors. Therefore, we can state that the binding affinities of the receptors are identical. Judging from the size change shown in Figure 2B, we can conclude that the increase in size is the essential factor for enhancing the cellular uptake. We can expect that, after internalization, the local concentration of CpG-ODN in the endosomal compartment should be higher than that of CpG/SPG. Since a higher concentration of ligands leads synergistically to an enhanced response in biological systems, the high

uptake may be better for adjuvant.

Lee et al. have demonstrated that multiple-glycoside binding to receptors on the cell surface drastically enhances binding affinity.[41] This is called the sugar-cluster effect and means that more binding sites normally allosterically result in more enhanced affinity.[42] The gel-network structure and increased molecular weight of CL-CpG may provide more binding sites than CpG/SPG. Furthermore, the morphology of the molecules plays a significant role in cellular uptake.[43] Given that anisotropic bacteria, such as those with a rod-like shape, are more likely to be taken up by cells, numerous researchers have developed drug carriers mimicking the bacterial morphology.[44] We assume that this morphological effect may also be involved in increasing the uptake of CL-CpG.

Further *in vitro* assays to optimize the adjuvant effects

Dependence of cytokine secretion on mixture composition

Single-stranded CpG-ODN is recognized by TLR9 in late endosomes.[15] The dsDNA BR assay shows almost no single-stranded CpG-ODN for CL-CpG (1:1). No dissociation of the double strands of CpG/cCpG by the breaking of crosslinks was observed at pH 5.5, which matches the conditions in late endosomes (see Figure S1).

Because of this, we assumed that CL-CpG (1:1) would not induce any biological response related to TLR9 and there would be an optimal composition other than 1:1 that is determined by comparing the uptake in Figure 1C and decreasing amount of single CpG chain upon changing the mixing ratio. Contrary to this expectation, the IL-6 secretion level peaked at a mixing ratio of 1:1, as shown in Figure 2. In the following experiments, we only used CL-CpG (1:1) for biological assays because of its highest uptake and cytokine secretion, suggesting that it has the most suitable composition for a beneficial adjuvant effect.

The result shown in Figure 2 was unexpected and thus a more detailed discussion may be needed because there is no single chain of CpG sequence that can bind to TLR9. According to recent studies,[45] there are various types of nucleic sensor other than TLR9 in APCs. Some of them bind to double-stranded non-immunogenic DNAs and induce immune responses. One possible explanation for the result of Figure 2 is that the highly concentrated DNA due to the high uptake of CL-CpG may interact with these DNA sensors. Another possibility is that this is still a TLR9-initiated response. We suppose that, when the concentration of CpG/cCpG double strands is increased in the endosomal compartment, the equilibrium between CpG/cCpG and CpG/TLR9 may be shifted toward CpG/TLR9 formation. This is simply because the competition between these two species follows the law of chemical equilibrium, namely, increased [CpG/cCpG] leads to the formation of CpG/TLR9. Nishikawa et al. found similar behavior for polypod-like structured DNA.[46] They exposed immune cells to polypod-shaped double-stranded DNA containing a CpG sequence and found that the polypod-shape enhanced uptake to induce the secretion of a large amount of cytokines. Later, they found that this event was triggered through TRL9.[47] Their result is also explained by the increased concentration of CpG double helix and then the equilibrium shift.[48]

Chemical structure of CpG-ODN backbone (PS or PO) and immune response

We examined how the difference between PS and PO affects IL-6 secretion, the results of which are presented in Figure 3. CL-CpG(PO) induced pronounced IL-6 secretion, which was almost five times greater than that of CpG(PO)/SPG. Contrary to PO, CL-CpG(PS) is lower than naked CpG(PS). It has been clearly demonstrated that TLR9 only binds to single-stranded DNAs that contain CpG portions and does not show any affinity to double-stranded DNA. We confirmed that CL-CpG(PO) and CL-CpG(PS)

have almost the same size and they are ingested by immune cells at the same levels. The large difference in the IL-6 secretion between them as shown in Figure 3 can be explained by two possible scenarios. First, the natural type PO double strands can be recognized by other DNA sensors,[49] but the PS ones cannot. Second, the PS sequence may form a less stable complex with TLR9 than that of PO[50] and, owing to this difference in stability, the formation of the TLR9/CpG(PO) complex can occur more frequently than that of TLR9/CpG(PS) when CpG double strands and TLR9/CpG are at equilibrium. Once the population of TLR9/CpG exceeds a certain critical concentration, the resultant biological response may be dramatically enhanced due to an allosteric effect. We have not obtained any results enabling us to draw conclusions on which of these reasons is more likely, but we only use CL-CpG(PO) in the subsequent analyses.

Adjuvant activity of CL-CpG nanogel

Figure 4A shows a comparison of the populations of OVA-specific CD8$^+$ cells when naked CpG, CpG/SPG or CL-CpG was injected as an adjuvant for OVA vaccine. CL-CpG induced more CTLs than the others, indicating that the co-administration of OVA and CL-CpG efficiently increased the population of CTL. Figure 4B more clearly demonstrates the enhanced CTL activity, indicating that the secretion of IFN-γ was dramatically increased only for CL-CpG. Here, IFN-γ secretion is one of the criteria for the formation of CD8$^+$ T cells. The cytokines including IFN-γ are called Th1 cell cytokines and induce macrophages and CTLs to attack tumor cells.

After the transplantation of E.G7-OVA cells that express OVA antigen on their surface into mice, we examined how CL-CpG+OVA prevents tumor growth (Figure 5A) and extends the survival of mice (Figure 5B), compared with CpG/SPG+OVA, CpG +OVA, and OVA alone. Figures 5A and 8B clearly demonstrate that CL-CpG+OVA is

markedly superior to the others. Incidentally, we had already shown that the strong CTL responses were created by CpG/SPG+OVA,[28,29] with the dose levels of ODN at 30 μg/head and OVA at 100 μg/head. In this study, compared with the previous ones, we decreased the dose level (ODN at 15 μg/head, OVA at 30 μg/head) because CL-CpG+OVA showed an excellent response at this low dose. However, the decreased dose may have caused a smaller difference between CpG/SPG+OVA and naked CpG+OVA. As we reported previously,[29] CpG/SPG+OVA improves the vaccine efficacy compared with CpG+OVA. We considered that this improvement is due to the APC targeting ability of CpG/SPG, while CpG has no such ability. CL-CpG showed further improvement compared with CpG/SPG. Presumably, this is related to its increased uptake, as shown in Figure 1.

Figures 5C and 5D present the dependence of tumor growth and survival on the CL-CpG dose. Despite some experimental error, we can conclude that CL-CpG+OVA vaccine is still effective even when the dose is reduced to 0.2 μg/head, where we fixed the OVA dose of 10 μg/head. Adjuvant efficacy of CpG-ODNs has been studied for the last 5 years and numerous papers on this topic have been published.[29] According to these previous studies, it is normally necessary to administer CpG at a dose of at least 30 μg/head. In these cases, CpG-ODNs were injected in a naked state. Compared with the efficacy at this dose, we achieved the same efficacy at almost one-hundredth of the dose. Additionally, in terms of the active adjuvant ingredient, our CpG contains 33.3 wt% of CpG in the total sequence. When we compared the efficacy on the basis of the CpG portion weight, 0.2 μg/head ODN corresponds to 0.07 μg/head CpG portion because our CpG-ODN has a dA40 tail. Therefore, again, to induce sufficient immunity, most previous studies[51-55] required CpG-ODN at more than 10 μg/head; compared with them, we can achieve similar immune responses at a far lower dose (i.e., 0.07 μg/head

CpG).

In our previous study, we observed IFN-α production upon the stimulation of human peripheral blood mononuclear cells with K-type CpG/SPG. Furthermore, we demonstrated that K-type CpG/SPG acted as an influenza vaccine adjuvant in a nonhuman primate model using cynomolgus monkey. Considering these findings, CL-CpG can be also applied to adjuvant for primate immunity, so it would be next issue to examine for primate, especially human, cancer model.

Numerous studies have focused on the conjugation of antigenic proteins to adjuvants.[54,55] Stayton et al. attached CpG to proteins and obtained a drastic enhancement of antigen-specific immune response.[56] However, the present study shows that such conjugation or encapsulation of antigenic proteins is not necessary because of the accumulation and activation of antigen-bearing macrophages and dendritic cells in the draining lymph node, as shown in our previous study.28 We can instead obtain better or equivalent efficacy than CpG-protein-conjugated vaccines simply by co-administering CL-CpG and OVA. We believe that this is a major advantage. For example, the chemical procedures to achieve conjugation are not required, and thus we do not have to perform purification or attempt to maximize the reaction yield for the conjugation. In addition, CL-CpG co-administration can be used for other vaccines such as for influenza to enhance their efficacy. This expansion of the range of applications is relatively easy because it only requires mixing of CL-CpG and vaccines.

III.4 Conclusions

We prepared a crosslinked nanogel consisting of CpG/SPG and cCpG/SPG complexes through hybridization between CpG and cCpG portions. The double-stranded CpG with PO induced a strong immune response, while those with PS did not. Immunization with

a mixture of CL-CpG and OVA induced antigen-specific CTL activities both in vitro and in vivo. These results can be attributed to the improved cellular uptake due to increased size, the cluster effect of the sugar recognition sites, and the subsequent high concentration of CpG-ODN in the endosomal compartment. Therefore, CL-CpG has great potential as a potent vaccine adjuvant for the treatment of cancers and infectious diseases.

III.5 Figures
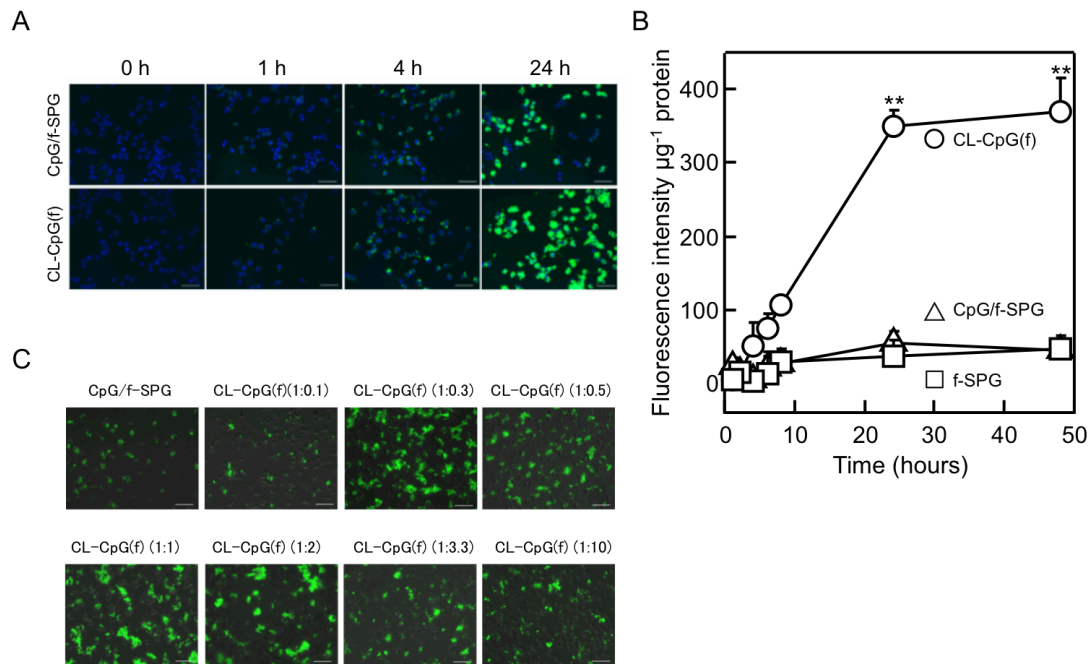
Figure 1. Uptake of CL-CpG into the RAW 264 cells. After adding CL-CpG(f) and CpG/f-SPG, the RAW 264 cells (A) were observed by fluorescence microscopy. The fluorescence intensities were plotted against time at the RAW 264 cells (n = 3)(B). **P < 0.01. The dependence of the level of FITC uptake on the CpG/f-SPG and cCpG/f-SPG mixing ratio with mice peritoneal macrophages is also presented, showing that the highest ingestion was obtained at a ratio of 1:1. (C)
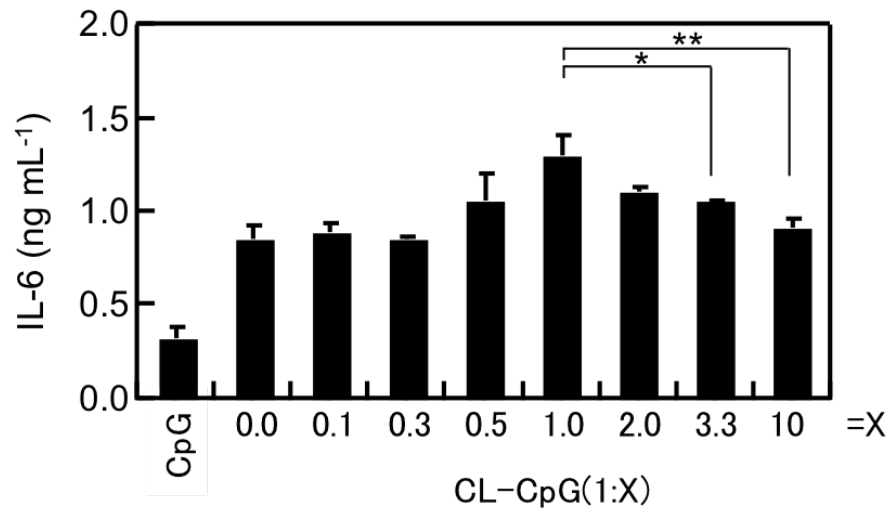
Figure 2. The dependence of IL-6 secretion on the CpG/SPG and cCpG/SPG mixing ratio in mouse splenocytes. *P < 0.05. **P < 0.01.
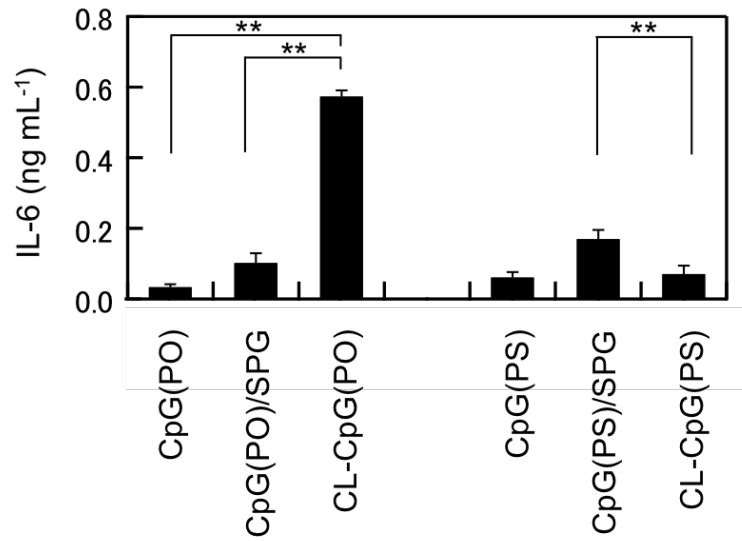
Figure 3. Different CpG-ODN backbones (PO and PS) and the IL-6 secretion response. The samples were added to mouse splenocytes at 200 nM. Results are presented as mean ± S.D. (n = 3). **P < 0.01.
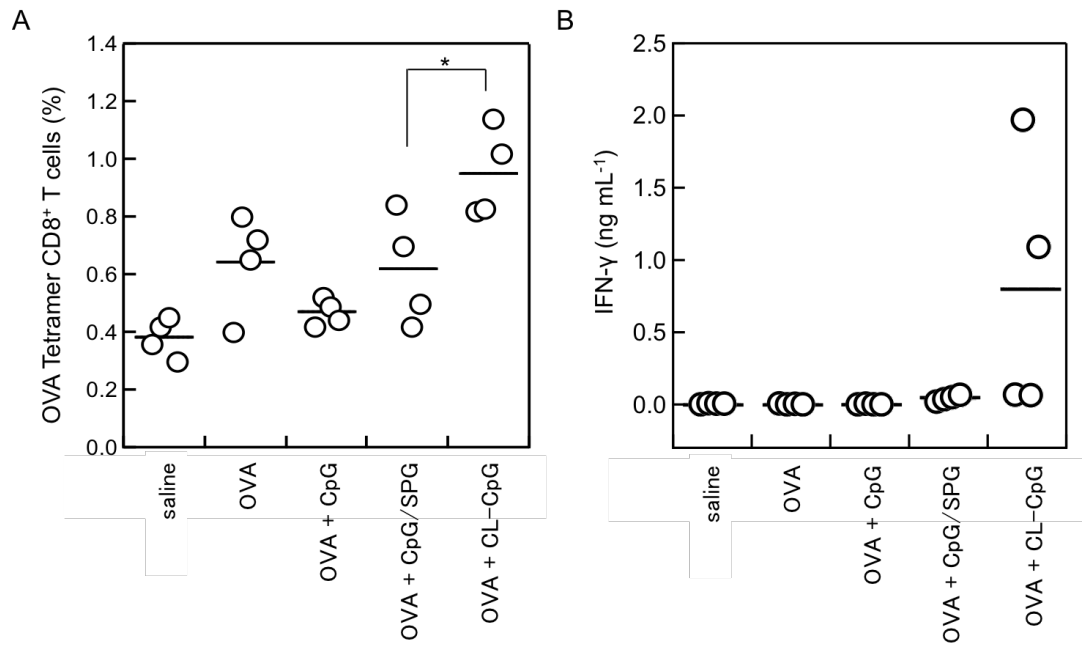
Figure 4. Induction of potent CTL activities by immunization with CL-CpG. OVA-specific CD8^{+} T cells (A) and IFN-γ production (B) were measured after immunization with OVA (30 µg/head) and the indicated adjuvants (A and B: ODN; 15 µg/head). Results are presented as mean ± S.D. ($n = 4$). *P < 0.05.
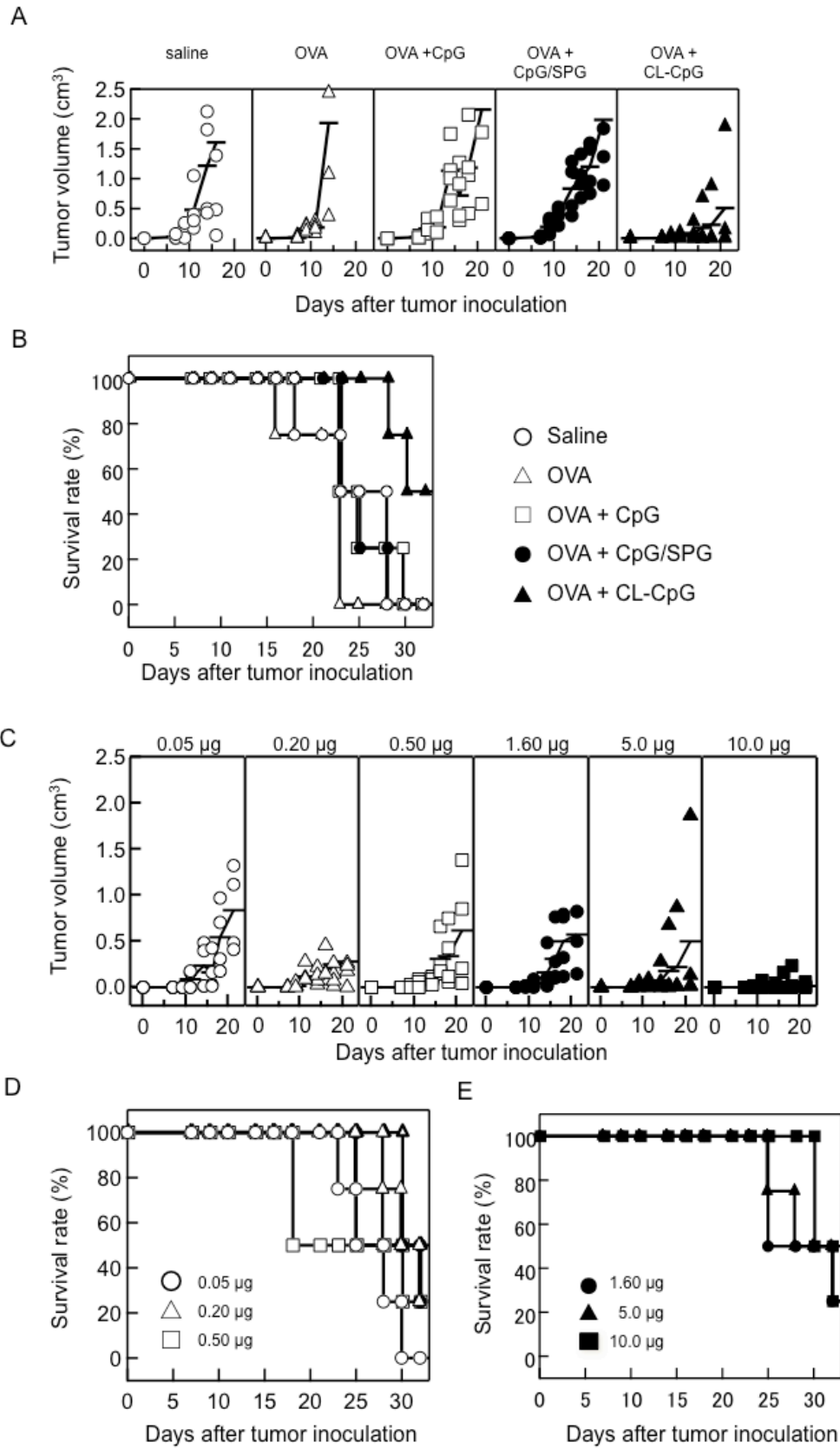
Figure 5. Immunization with a mixture of CL-CpG and OVA to suppress tumor growth.

Before translated OVA peptide-bearing tumor cells, on days −17 and −7, mice were

immunized with OVA (10 μg/head) and the indicated adjuvants (ODN; 5.0 μg/head).

Changes in tumor volume (A) and mortality (B) were monitored after tumor inoculation

(n = 4). Upon immunization with OVA (10 μg/head) and CL-CpG (ODN; 0.05, 0.20,

0.50, 1.60, 5.0, or 10 μg/head), changes in tumor volume (C) and mortality (D, E) were

monitored after tumor inoculation (n = 4).

1 CpG
2 CpG/SPG
3 CL-CpG pH7.5
4 CL-CpG pH7.0
5 CL-CpG pH6.5
6 CL-CpG pH6.0
7 CL-CpG pH5.0
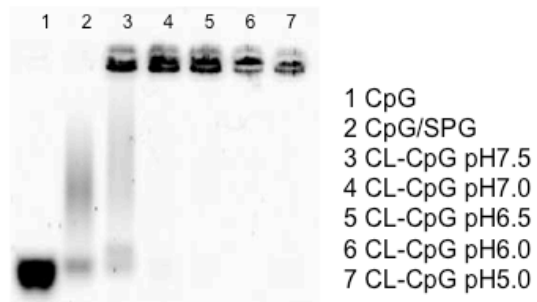
Figure S1. The stability of CL-CpG under conditions matching those in late endosomes. The CL-CpG was incubated at the indicated pH for 1 h and subjected to agarose gel electrophoresis.

III.6 References

(1)   Couzin-Frankel, J. (2013) Cancer immunotherapy. *Science 342*, 1432-1433.

(2)   Schumacher, T. N., and Schreiber, R. D. (2015) Neoantigens in cancer immunotherapy. *Science 348*, 69-74.

(3)   Pardoll, D. M. (2012) The blockade of immune checkpoints in cancer immunotherapy. *Nature Reviews Cancer 12*, 252-264.

(4)   Sadelain, M., Brentjens, R., and Rivière, I. (2009) The promise and potential pitfalls of chimeric antigen receptors. *Current opinion in immunology 21*, 215-223.

(5)   Purcell, A. W., McCluskey, J., and Rossjohn, J. (2007) More than one reason to rethink the use of peptides in vaccine design. *Nature reviews Drug discovery 6*, 404-414.

(6)   Rosenberg, S. A., Yang, J. C., and Restifo, N. P. (2004) Cancer immunotherapy: moving beyond current vaccines. *Nature medicine 10*, 909-915.

(7)   Yoshiyuki, Y. (2016) Immunotherapy of Cancer.

(8)   van der Burg, S. H., Arens, R., Ossendorp, F., van Hall, T., and Melief, C. J. M. (2016) Vaccines for established cancer: overcoming the challenges posed by immune evasion. *Nature Reviews Cancer 16*, 219-233.

(9)   Muraoka, D., Harada, N., Hayashi, T., Tahara, Y., Momose, F., Sawada, S.-i., Mukai, S.-a., Akiyoshi, K., and Shiku, H. (2014) Nanogel-based immunologically stealth vaccine targets macrophages in the medulla of lymph node and induces potent antitumor immunity. *ACS nano 8*, 9209-9218.

(10)   Germain, R. N. (1994) MHC-dependent antigen processing and peptide presentation: providing ligands for T lymphocyte activation. *Cell 76*, 287-299.

(11)   Huang, A., Golumbek, P., Ahmadzadeh, M., Jaffee, E., Pardoll, D., and Levitsky, H. (1994) Role of bone marrow-derived cells in presenting MHC class I-restricted tumor antigens. *Science 264*, 961-965.

(12)   Takeuchi, O., and Akira, S. (2010) Pattern recognition receptors and inflammation. *Cell 140*, 805-820.

(13)   Desmet, C. J., and Ishii, K. J. (2012) Nucleic acid sensing at the interface between innate and adaptive immunity in vaccination. *Nat Rev Immunol 12*, 479-491.

(14)   Savva, A., and Roger, T. (2013) Targeting toll-like receptors: promising therapeutic strategies for the management of sepsis-associated pathology and infectious diseases. *Front Immunol 4*, 387.

(15)   Hemmi, H., Takeuchi, O., Kawai, T., Kaisho, T., Sato, S., Sanjo, H., Matsumoto, M., Hoshino, K., Wagner, H., and Takeda, K. (2000) A Toll-like receptor recognizes bacterial DNA. *Nature 408*, 740-745.

(16)   Bauer, S., Kirschning, C. J., Häcker, H., Redecke, V., Hausmann, S., Akira, S., Wagner, H., and Lipford, G. B. (2001) Human TLR9 confers responsiveness to bacterial DNA via species-specific CpG motif recognition. *Proceedings of the National Academy of Sciences 98*, 9237-9242.

(17)   Krieg, A. M., Yi, A.-K., Matson, S., Waldschmidt, T. J., Bishop, G. A., Teasdale, R., Koretzky, G. A., and Klinman, D. M. (1995) CpG motifs in bacterial DNA trigger direct B-cell activation. *Nature 374*, 546-549.

(18)   Krieg, A. M., PW, D., ME, A., S, A., CC, G., and DT, F. (2002) CPG MOTIFS IN BACTERIAL DNA AND THEIR IMMUNE EFFECTS

C3d of complement as a molecular adjuvant: bridging innate and acquired immunity. *Annual Review of Immunology 20*, 709-760.

(19)   Verthelyi, D., Ishii, K. J., Gursel, M., Takeshita, F., and Klinman, D. M. (2001) Human peripheral blood cells differentially recognize and respond to two distinct CPG motifs. *The Journal of Immunology 166*, 2372-2377.

(20)   Wu, C. C., Lee, J., Raz, E., Corr, M., and Carson, D. A. (2004) Necessity of oligonucleotide aggregation for toll-like receptor 9 activation. *Journal of Biological Chemistry 279*, 33071-33078.

(21)   Puig, M., Grajkowski, A., Boczkowska, M., Ausín, C., Beaucage, S. L., and Verthelyi, D. (2006) Use of thermolytic protective groups to prevent G-tetrad formation in CpG ODN type D: structural studies and immunomodulatory activity in primates. *Nucleic acids research 34*, 6488-6495.

(22)   Aoshi, T., Haseda, Y., Kobiyama, K., Narita, H., Sato, H., Nankai, H., Mochizuki, S., Sakurai, K., Katakai, Y., Yasutomi, Y., et al. (2015) Development of Nonaggregating Poly-A Tailed Immunostimulatory A/D Type CpG Oligodeoxynucleotides Applicable for Clinical Use. *J Immunol Res 2015*, 316364.

(23)   Krug, A., Rothenfusser, S., Hornung, V., Jahrsdörfer, B., Blackwell, S., Ballas, Z. K., Endres, S., Krieg, A. M., and Hartmann, G. (2001) Identification of CpG oligonucleotide sequences with high induction of IFN‐α/β in plasmacytoid dendritic cells. *European journal of immunology 31*, 2154-2163.

(24) Krieg, A. M. (2002) CPG motifs in bacterial dna and their immune effects*. *Annual review of immunology 20,* 709-760.

(25) Iannitti, T., Cesar Morales-Medina, J., and Palmieri, B. (2014) Phosphorothioate oligonucleotides: effectiveness and toxicity. *Current drug targets 15,* 663-673.

(26) Minari, J., Mochizuki, S., Matsuzaki, T., Adachi, Y., Ohno, N., and Sakurai, K. (2011) Enhanced cytokine secretion from primary macrophages due to Dectin-1 mediated uptake of CpG DNA/beta-1,3-glucan complex. *Bioconjugate chemistry 22,* 9-15.

(27) Miyamoto, N., Mochizuki, S., and Sakurai, K. (2014) Enhanced Immunostimulation with Crosslinked CpG-DNA/^|^beta;-1,3-Glucan Nanoparticle through Hybridization. *Chemistry Letters 43,* 991-993.

(28) Kobiyama, K., Aoshi, T., Narita, H., Kuroda, E., Hayashi, M., Tetsutani, K., Koyama, S., Mochizuki, S., Sakurai, K., Katakai, Y., et al. (2014) Nonagonistic Dectin-1 ligand transforms CpG into a multitask nanoparticulate TLR9 agonist. *Proc Natl Acad Sci U S A 111,* 3086-3091.

(29) Mochizuki, S., Morishita, H., Kobiyama, K., Aoshi, T., Ishii, K. J., and Sakurai, K. (2015) Immunization with antigenic peptides complexed with beta-glucan induces potent cytotoxic T-lymphocyte activity in combination with CpG-ODNs. *J Control Release 220,* 495-502.

(30) Sakurai, K., and Shinkai, S. (2000) Molecular Recognition of Adenine, Cytosine, and Uracil in a Single-Stranded RNA by a Natural Polysaccharide: Schizophyllan. *Journal of the American Chemical Society 122,* 4520-4521.

(31) Serda, R. E. (2013) Particle platforms for cancer immunotherapy. *Int J*

Nanomedicine 8, 1683-1696.

(32) Irvine, D. J., Hanson, M. C., Rakhra, K., and Tokatlian, T. (2015) Synthetic Nanoparticles for Vaccines and Immunotherapy. *Chem Rev 115*, 11109-11146.

(33) Li, Y., Lian, Y., Zhang, L. T., Aldousari, S. M., Hedia, H. S., Asiri, S. A., and Liu, W. K. (2016) Cell and nanoparticle transport in tumour microvasculature: the role of size, shape and surface functionality of nanoparticles. *Interface Focus 6*, 20150086.

(34) Manolova, V., Flace, A., Bauer, M., Schwarz, K., Saudan, P., and Bachmann, M. F. (2008) Nanoparticles target distinct dendritic cell populations according to their size. *Eur J Immunol 38*, 1404-1413.

(35) Mochizuki, S., and Sakurai, K. (2010) beta-1,3-Glucan/antisense oligonucleotide complex stabilized with phosphorothioation and its gene suppression. *Bioorg Chem 38*, 260-264.

(36) Mizu, M., Koumoto, K., Anada, T., Karinaga, R., Kimura, T., Nagasaki, T., Shinkai, S., and Sakurai, K. (2004) Enhancement of the antisense effect of polysaccharide-polynucleotide complexes by preventing the antisense oligonucleotide from binding to proteins in the culture medium. *Bulletin of the Chemical Society of Japan 77*, 1101-1110.

(37) Hasegawa, T., Fujisawa, T., Numata, M., Umeda, M., Matsumoto, T., Kimura, T., Okumura, S., Sakurai, K., and Shinkai, S. (2004) Single-walled carbon nanotubes acquire a specific lectin-affinity through supramolecular wrapping with lactose-appended schizophyllan. *Chemical communications*, 2150-2151.

(38) Brown, G. D., and Gordon, S. (2001) Immune recognition: A new receptor for

[beta]-glucans. *Nature 413*, 36-37.

(39)   Brown, G. D., Taylor, P. R., Reid, D. M., Willment, J. A., Williams, D. L., Martinez-Pomares, L., Wong, S. Y., and Gordon, S. (2002) Dectin-1 is a major beta-glucan receptor on macrophages. *The Journal of experimental medicine 196*, 407-412.

(40)   Mochizuki, S., Morishita, H., Adachi, Y., Yamaguchi, Y., and Sakurai, K. (2014) Binding assay between murine Dectin-1 and β-glucan/DNA complex with quartz-crystal microbalance. *Carbohydrate research 391*, 1-8.

(41)   Lee, Y. C., and Lee, R. T. (1995) Carbohydrate-Protein Interactions: Basis of Glycobiology. *Accounts of Chemical Research 28*, 321-327.

(42)   Mammen, M., Choi, S.-K., and Whitesides, G. M. (1998) Polyvalent interactions in biological systems: implications for design and use of multivalent ligands and inhibitors. *Angewandte Chemie International Edition 37*, 2754-2794.

(43)   Gratton, S. E., Ropp, P. A., Pohlhaus, P. D., Luft, J. C., Madden, V. J., Napier, M. E., and DeSimone, J. M. (2008) The effect of particle design on cellular internalization pathways. *Proc Natl Acad Sci U S A 105*, 11613-11618.

(44)   Mitragotri, S., and Lahann, J. (2009) Physical approaches to biomaterial design. *Nat Mater 8*, 15-23.

(45)   Paludan, S. R., and Bowie, A. G. (2013) Immune sensing of DNA. *Immunity 38*, 870-880.

(46)   Mohri, K., Nishikawa, M., Takahashi, N., Shiomi, T., Matsuoka, N., Ogawa, K., Endo, M., Hidaka, K., Sugiyama, H., and Takahashi, Y. (2012) Design and development of nanosized DNA assemblies in polypod-like structures as

efficient vehicles for immunostimulatory CpG motifs to immune cells. *ACS nano 6*, 5931-5940.

(47)   Uno, S., Nishikawa, M., Mohri, K., Umeki, Y., Matsuzaki, N., Takahashi, Y., Fujita, H., Kadowaki, N., and Takakura, Y. (2014) Efficient delivery of immunostimulatory DNA to mouse and human immune cells through the construction of polypod-like structured DNA. *Nanomedicine: Nanotechnology, Biology and Medicine 10*, 765-774.

(48)   Sanada, Y., Shiomi, T., Okobira, T., Tan, M., Nishikawa, M., Akiba, I., Takakura, Y., and Sakurai, K. (2016) Polypod-Shaped DNAs: Small-Angle X-ray Scattering and Immunostimulatory Activity. *Langmuir 32*, 3760-3765.

(49)   Kim, D., Rhee, J. W., Kwon, S., Sohn, W.-J., Lee, Y., Kim, D.-W., Kim, D.-S., and Kwon, H.-J. (2009) Immunostimulation and anti-DNA antibody production by backbone modified CpG-DNA. *Biochemical and biophysical research communications 379*, 362-367.

(50)   Ohto, U., Shibata, T., Tanji, H., Ishida, H., Krayukhina, E., Uchiyama, S., Miyake, K., and Shimizu, T. (2015) Structural basis of CpG and inhibitory DNA recognition by Toll-like receptor 9. *Nature 520*, 702-705.

(51)   Gungor, B., Yagci, F. C., Tincer, G., Bayyurt, B., Alpdundar, E., Yildiz, S., Ozcan, M., Gursel, I., and Gursel, M. (2014) CpG ODN nanorings induce IFNα from plasmacytoid dendritic cells and demonstrate potent vaccine adjuvant activity. *Science translational medicine 6*, 235ra261-235ra261.

(52)   Kim, J., Li, W. A., Choi, Y., Lewin, S. A., Verbeke, C. S., Dranoff, G., and Mooney, D. J. (2015) Injectable, spontaneously assembling, inorganic scaffolds modulate immune cells in vivo and increase vaccine efficacy. *Nature*

biotechnology 33, 64-72.

(53)   Yildiz, S., Alpdundar, E., Gungor, B., Kahraman, T., Bayyurt, B., Gursel, I., and Gursel, M. (2015) Enhanced immunostimulatory activity of cyclic dinucleotides on mouse cells when complexed with a cell-penetrating peptide or combined with CpG. *Eur J Immunol 45*, 1170-1179.

(54)   de Jong, S., Chikh, G., Sekirov, L., Raney, S., Semple, S., Klimuk, S., Yuan, N., Hope, M., Cullis, P., and Tam, Y. (2007) Encapsulation in liposomal nanoparticles enhances the immunostimulatory, adjuvant and anti-tumor activity of subcutaneously administered CpG ODN. *Cancer Immunol Immunother 56*, 1251-1264.

(55)   Lee, Y. R., Lee, Y. H., Kim, K. H., Im, S. A., and Lee, C. K. (2013) Induction of Potent Antigen-specific Cytotoxic T Cell Response by PLGA-nanoparticles Containing Antigen and TLR Agonist. *Immune Netw 13*, 30-33.

(56)   Wilson, J. T., Keller, S., Manganiello, M. J., Cheng, C., Lee, C. C., Opara, C., Convertine, A., and Stayton, P. S. (2013) pH-Responsive nanoparticle vaccines for dual-delivery of antigens and immunostimulatory oligonucleotides. *ACS nano 7*, 3912-3925.

Chapter IV

A beta-glucan/ODN carrier conjugated with TAT peptide: Specific delivery to cytosol

IV-1 Introduction

Antisense oligonucleotides (ASOs) are single-stranded nucleic acids consisting of 15–25 nucleotides in length, which bind to the target mRNA sequence specifically, resulting in interference with gene expression. ASOs can modulate gene expression by several mechanisms including RNase H-mediated degradation of the target RNA[1,2] or skipping of the targeted exon and altering the RNA and protein sequence.[3] One of the major obstacles for clinical application of ASOs is enzymatic degradation in vivo. From first introduction by Zamecnik et al.,[4] chemical modifications to the backbone have been at the center of research interest for improvement of stability in vivo. Among chemical modifications, phosphorothioate (PS) backbone that replaced one of the nonbridging oxygen atoms in the phosphodiester backbone with a sulfur atom is termed the first generation of oligonucleotide modifications and reported to show a high stability in serum.[5] Despite the benefit, there is room for consideration of cellular uptake. Thus, the efficient and non-toxic delivery systems have been developed by many groups, including liposomes and cationic polymer complexes. In our previous study, we have found oligonucleotide (ODN) delivery system by complex of polysaccharide Schizophyllan (SPG) and ODN. Our group have studied a beta glucan, Schizophyllan, in short, SPG as a ODN carrier. When SPG in alkaline solution is neutralized with some of single chain homopolynucleotides such as poly deoxyadenylic acid (polydA) forms ODN/SPG complex. [6,7] In particular, PS-polydA is a stronger binding affinity to SPG than phosphodiester (PO) backbone-polydA.[8] The SPG is one of beta-glucan and recognized Dectin-1 of beta-glucan receptor. We have demonstrated that Dectin-1 recognizes SPG/ODN complexes and shows a high stability in serum,[9] and the complex is eventually ingested by the cells and transports functional ODN including antisense (AS)-ODN, CpG-ODN, and siRNA to expressed Dectin-1 cells.[10-13]

Among the various proposed delivery carriers, cell-penetrating peptides (CPPs) have much attention as the most promising carrier for internalization into cells.[14]

Ryser and his colleagues first demonstrated that conjugation of cationic peptides to anticancer drugs can improve cellular uptake in vitro and in vivo.[15] Most CPPs, small and basic amino acids-rich peptide as shown in HIV-1 Tat protein, are found to have the ability to translocate across cellular plasma membranes.[16,17] Therefore they are often used by covalent conjugation with drugs or drug-embedded carriers. In case of conjugation with oligonucleotides (ODNs), a disulfide, ester and peptide bonds are employed. Among the conjugations, a disulfide bond between peptide with cysteine residue and maleimidemodified ODNs is largely advantageous because a disulfide linkage is dissociated in the reducing milieu, resulting in release of ODN from peptide.[18] Although there are many reports concerning the synthesis of peptide-ODN conjugates (POCs) comprising a peptide and an ODN with phosphodiester backbones, only few papers describe the preparation of POCs with PS backbones (POCPs).[19] Since the ODNs with PS backbones can induce a side react with a peptide bearing a disulfide reactive functional group, it is difficult to purify and evaluate the characterization of POCPs linked at the desired sites. Azhayev and his colleagues reported well-characterized POCPs using a PS-ODN with a mercaptoalkyl group and a peptide with a pyridyl disulfide function.[20] 'Click Chemistry' is a concept of chemical reaction introduced by Sharpless at el. in 2001.[21] Azide alkyne Huisgen cycloaddition using a copper catalyst is one of the most popular reactions and can be proceeded in benign reaction conditions and give high yields.[22] In study, we synthesized POCPs with a simple reaction, where the POCPs comprise one of the major CPPs, Tat peptide, and PS-modified dA_{40} (PS-dA_{40}) and formed with SPG/AS-ODN complex. The SPG/ODN/POCPs was observed into cytosol and examined the inhibition effect of cell

growth by treatment with AS-ODN for four human EGF receptor3 (HER3) that is good

targeting for cancer therapy.[23]

IV-Results and Discussions

We prepared PS-dA$_{40}$ with alkyne group at 50-terminus and Tat peptide with azide group at C-terminus (Fig. 1A), and mixed the both compounds at various molar ratios with copper catalyst for the optimization of reaction condition. After the reaction, we soon added a chelate agent ethylenediaminetetraacetic acid (EDTA) to prevent the aggregations because PS-dA$_{40}$ is considered to be easy to crosslink via cupper molecules. To confirm the conjugation, the reaction mixture was analyzed with high-performance liquid chromatography (HPLC). (Fig. 1B) From the chromatograms monitored by UV absorbance at 260 nm before and after the reaction, the peak of PS-dA$_{40}$ shifted to an earlier elution time, indicating the increment in hydrophilicity of PS-dA$_{40}$ by conjugation with Tat peptide (Tat-dA$_{40}$).

Figure 2 compares the gel permeation chromatograms (GPC) for Tat-dA$_{40}$ with ODN/SPG complex. Here, only nucleotides (i.e., Alexa 546 modified-dA$_{40}$ (Ale or Ale-dA$_{40}$)) can be detected at 22 min. The complexation samples caused the UV peak at 260 and 546 nm to shift from 20 to 15 min. At the UV at 260 nm, all ODNs were detected. On the other hand, the Ale-dA$_{40}$ was detected at UV at 546 nm. At the calculated Tat-dA$_{40}$ ratio in a complex, the molar of Tat-dA$_{40}$ followed the change amount. (Table1)

Figure 3A. shows uptake and localization of TAT complex in PC9 cell, a human lung cancer cell line. The PC9 is expressing Dectin-1 of beta glucan receptor. The Tat/FITC –modified dA$_{40}$ (FITC)/SPG (0:7:2) and (5:2:2) were observed the fluorescence at indicated 8 and 24 hours. Then the two complexes were added at the same concentration. The green shows FITC-modified dA$_{40}$ and blue are nuclear stained by DAPI. Tat/ FITC/SPG (5:2:2) was taken up by the cells in a time-dependent manner. At 24 hours, the fluorescence of Tat/ FITC/SPG (5:2:2) was higher than Tat/ FITC/SPG (0:7:2). This

result indicates TAT peptide certainly promotes the internalization to cells.

Some papers reported TAT peptide acts to go to nuclear. So we mainly observed localization of TAT complex around nuclear. Figure 3B. was observed line scanning profiles, Tat/ FITC/SPG (0:7:2) and Tat/ FITC/SPG (5:2:2) does not overlap with DAPI. The ODN/SPG complex with TAT exists in cytosol, not nuclear.

Figure 4 shows the cell proliferation rates after treatment with Tat/dA$_{40}$/AS-HER3/SPG. The treatment with Tat/dA$_{40}$/AS-HER3/SPG (5:0:2:2) suppressed the cell proliferation of PC9 cells, while that with the naked AS-HER3 and other samples did not show any suppression. The result suggests that Tat peptides of Tat/dA$_{40}$/AS-HER3/SPG can improve the cellular uptake to cytosol and suppress the target gene expression.

IV-3 Conclusions

In the field of drug development, the application of Click Chemistry is increasing for exploration of useful compounds. The most of the researches use the reaction concerning the formation of a tria-zole ring by use of copper catalyst. In this study, We prepared Tat peptide conjugate phosphorothioate dA_{40} oligonucleotide (Tat-dA_{40}) by the click chemistry reaction. The Tat-dA40/AS-HER3/SPG complexes showed a higher cell uptake and more cell-growth suppression than AS-HER3/SPG complex that had not Tat. We suppose that this improvement can be ascribed to Tat-induced cellular ingestion of the complexes.

IV-4 Figures

A

| Azide-modified Tat peptide | Alkyne-modified PS-dA$_{40}$ | Tat-dA$_{40}$ |

B
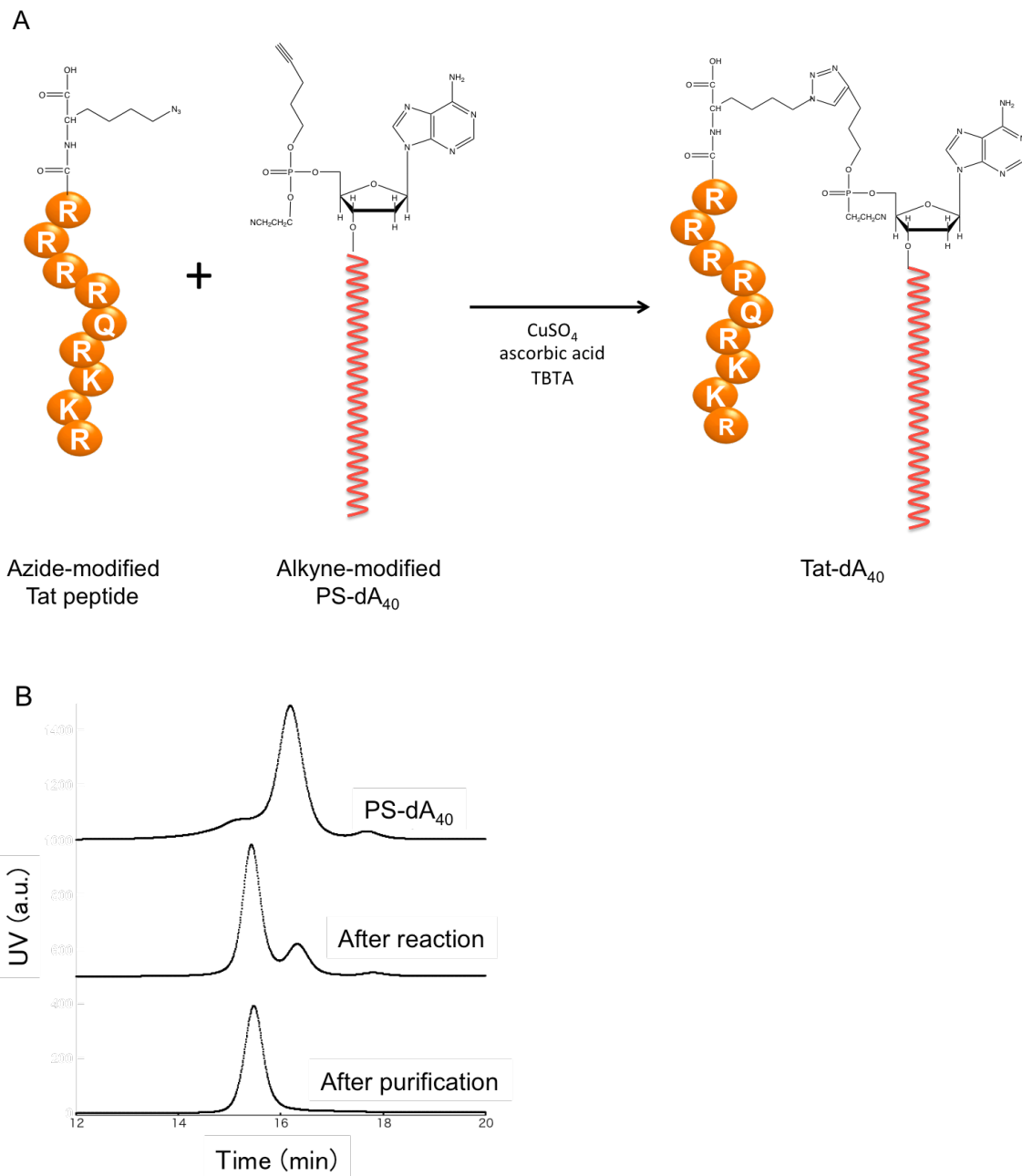
Figure 1. (A) Synthesis of Tat-dA$_{40}$: click chemistry reaction. (B) Confirmation of the conjugation between alkyne-modified PS-dA$_{40}$ and azide-modified Tat peptide, and purification of the conjugate by HPLC.
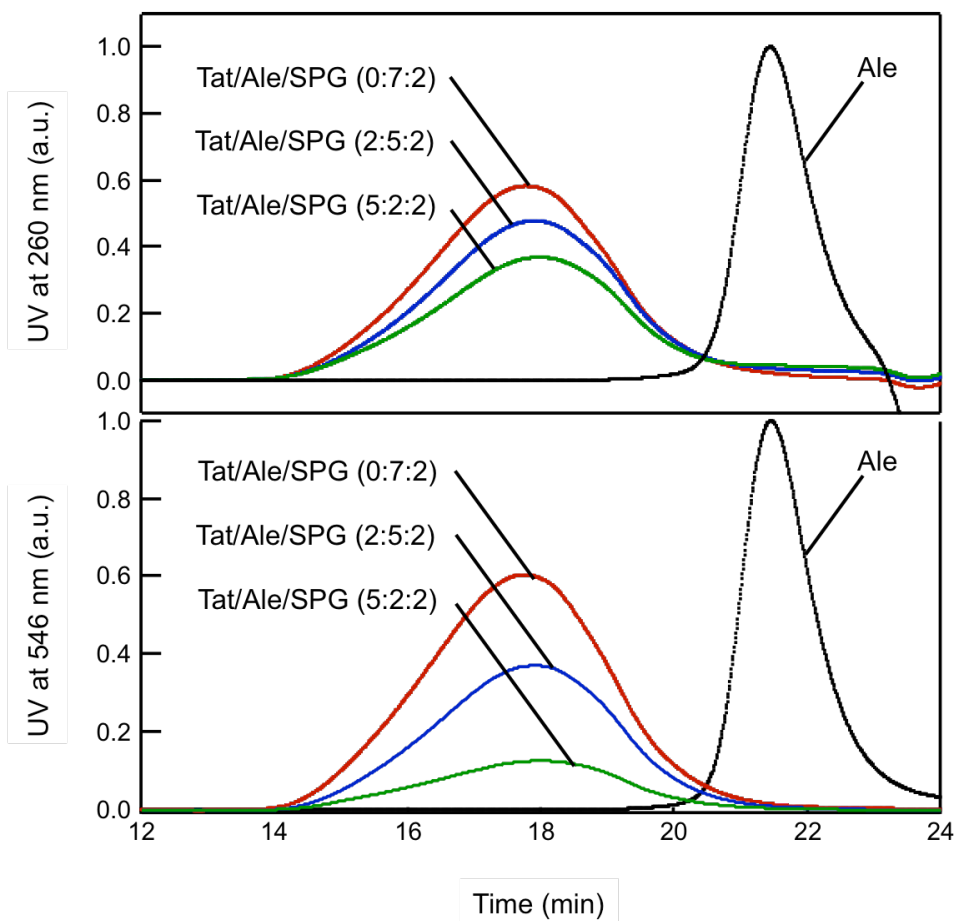
Figure 2. Confirmation of the complex at changing molar ratio between Tat-dA$_{40}$ and ODN in SPG were detected by GPC.

Table 1. The molar ratio of Tat-dA40 and Ale-dA40 in SPG

	Tat/Ale/SPG (0:7:2)	Tat/Ale/SPG (2:5:2)	Tat/Ale/SPG (5:2:2)
Tat-dA$_{40}$ (mol)	0	1.1	4.7
Ale-dA$_{40}$ (mol)	6.7	5.9	2.3

$*[\text{TAT-dA}_{40}]=[\text{Total ODN}_{260\text{ nm}}]- [\text{Ale-dA}_{40\text{ }546\text{nm}}]$

89

Figure 3. (A) Uptake of Tat/FITC-modified-dA$_{40}$(FITC)/SPG into the PC9 cells. After adding Tat/FITC/SPG, the PC9 cells (A) were observed by fluorescence microscopy and (B) detected the line scanning of cell.
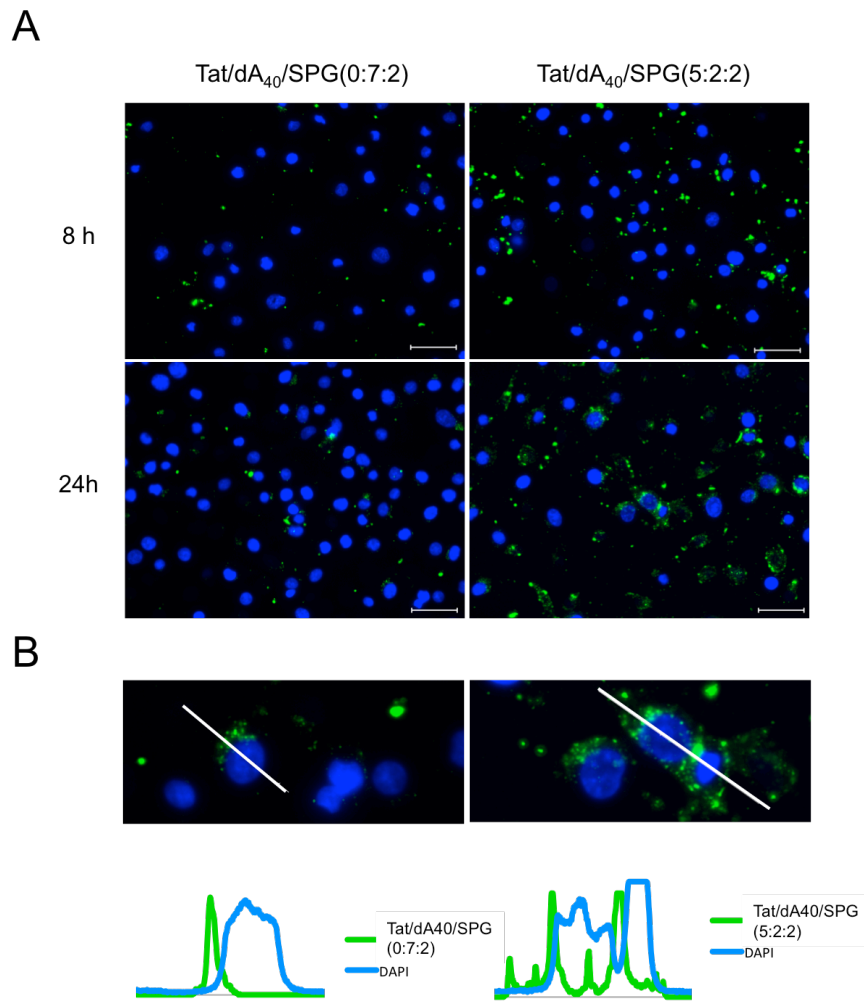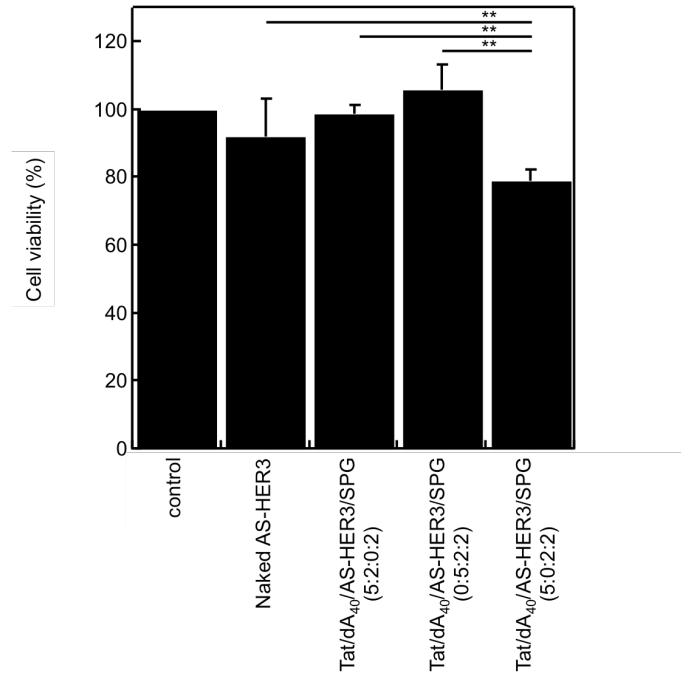
Figure 4. Inhibition of cell proliferation by treatment with Naked AS-HER3, Tat/dA$_{40}$/AS-HER3/SPG(5:2:0:2), (0:5:2:2), and (5:0:2:2). Results represent the mean ± SD (n = 3). **P < 0.01.

IV-5 References

(1)   Stanley, T. C. (2004) Antisense Strategies. *Current Molecular Medicine 4*, 465-487.

(2)   Stein, H., and Hausen, P. (1969) Enzyme from calf thymus degrading the RNA moiety of DNA-RNA Hybrids: effect on DNA-dependent RNA polymerase. *Science 166*, 393-395.

(3)   Zalachoras, I., Grootaers, G., van Weert, L. T., Aubert, Y., de Kreij, S. R., Datson, N. A., van Roon-Mom, W. M., Aartsma-Rus, A., and Meijer, O. C. (2013) Antisense-mediated isoform switching of steroid receptor coactivator-1 in the central nucleus of the amygdala of the mouse brain. *BMC Neuroscience 14*, 5.

(4)   Stephenson, M. L., and Zamecnik, P. C. (1978) Inhibition of Rous sarcoma viral RNA translation by a specific oligodeoxyribonucleotide. *Proceedings of the National Academy of Sciences 75*, 285-288.

(5)   Campbell, J. M., Bacon, T. A., and Wickstrom, E. (1990) Oligodeoxynucleoside phosphorothioate stability in subcellular extracts, culture media, sera and cerebrospinal fluid. *Journal of biochemical and biophysical methods 20*, 259-267.

(6)   Sakurai, K., and Shinkai, S. (2000) Molecular Recognition of Adenine, Cytosine, and Uracil in a Single-Stranded RNA by a Natural Polysaccharide: Schizophyllan. *Journal of the American Chemical Society 122*, 4520-4521.

(7)   Sakurai, K., Mizu, M., and Shinkai, S. (2001) Polysaccharide−Polynucleotide Complexes. 2. Complementary Polynucleotide Mimic Behavior of the Natural Polysaccharide Schizophyllan in the Macromolecular Complex with Single-Stranded RNA and DNA. *Biomacromolecules 2*, 641-650.

(8)   Mochizuki, S., and Sakaurai, K. (2010) β-1, 3-Glucan/antisense oligonucleotide complex stabilized with phosphorothioation and its gene suppression. *Bioorganic chemistry 38*, 260-264.

(9)   Minari, J., Mochizuki, S., Matsuzaki, T., Adachi, Y., Ohno, N., and Sakurai, K. (2011) Enhanced cytokine secretion from primary macrophages due to Dectin-1 mediated uptake of CpG DNA/beta-1,3-glucan complex. *Bioconjug Chem 22*, 9-15.

(10)   Mochizuki, S., and Sakurai, K. (2011) Dectin-1 targeting delivery of TNF-alpha antisense ODNs complexed with beta-1,3-glucan protects mice from LPS-induced hepatitis. *J Control Release 151*, 155-161.

(11)   Mochizuki, S., Morishita, H., and Sakurai, K. (2013) Macrophage specific delivery of TNF-alpha siRNA complexed with beta-1,3-glucan inhibits LPS-induced cytokine production in a murine acute hepatitis model. *Bioorg Med Chem 21*, 2535-2542.

(12)   Kobiyama, K., Aoshi, T., Narita, H., Kuroda, E., Hayashi, M., Tetsutani, K., Koyama, S., Mochizuki, S., Sakurai, K., Katakai, Y., et al. (2014) Nonagonistic Dectin-1 ligand transforms CpG into a multitask nanoparticulate TLR9 agonist. *Proc Natl Acad Sci U S A 111*, 3086-3091.

(13)   Miyamoto, N., Mochizuki, S., and Sakurai, K. (2014) Enhanced Immunostimulation with Crosslinked CpG-DNA/^|^beta;-1,3-Glucan

Nanoparticle through Hybridization. *Chemistry Letters 43*, 991-993.

(14)   Margus, H., Padari, K., and Pooga, M. (2012) Cell-penetrating peptides as versatile vehicles for oligonucleotide delivery. *Molecular Therapy 20*, 525-533.

(15)   Ryser, H. J.-P., and Shen, W.-C. (1978) Conjugation of methotrexate to poly(L-lysine) increases drug transport and overcomes drug resistance in cultured cells. *Proceedings of the National Academy of Sciences 75*, 3867-3870.

(16)   Frankel, A. D., and Pabo, C. O. (1988) Cellular uptake of the tat protein from human immunodeficiency virus. *Cell 55*, 1189-1193.

(17)   Brooks, H., Lebleu, B., and Vivès, E. (2005) Tat peptide-mediated cellular delivery: back to basics. *Advanced drug delivery reviews 57*, 559-577.

(18)   Muratovska, A., and Eccles, M. R. (2004) Conjugate for efficient delivery of short interfering RNA (siRNA) into mammalian cells. *FEBS letters 558*, 63-68.

(19)   Chaloin, L., Vidal, P., Lory, P., Mery, J., Lautredou, N., Divita, G., and Heitz, F. (1998) Design of carrier peptide-oligonucleotide conjugates with rapid membrane translocation and nuclear localization properties. *Biochemical and biophysical research communications 243*, 601-608.

(20)   Antopolsky, M., Azhayeva, E., Tengvall, U., Auriola, S., Jääskeläinen, I., Rönkkö, S., Honkakoski, P., Urtti, A., Lönnberg, H., and Azhayev, A. (1999) Peptide−Oligonucleotide Phosphorothioate Conjugates with Membrane Translocation and Nuclear Localization Properties. *Bioconjugate Chemistry 10*, 598-606.

(21)   Kolb, H. C., Finn, M., and Sharpless, K. B. (2001) Click chemistry: diverse chemical function from a few good reactions. *Angewandte Chemie International*

Edition 40, 2004-2021.

(22)   Spiteri, C., and Moses, J. E. (2010) Copper Catalyzed Azide–Alkyne
         Cycloaddition: Regioselective Synthesis of 1, 4, 5 Trisubstituted 1, 2, 3
         Triazoles. *Angewandte Chemie International Edition 49*, 31-33.

(23)   Gaborit, N., Abdul-Hai, A., Mancini, M., Lindzen, M., Lavi, S., Leitner, O.,
         Mounier, L., Chentouf, M., Dunoyer, S., and Ghosh, M. (2015) Examination of
         HER3 targeting in cancer using monoclonal antibodies. *Proceedings of the
         National Academy of Sciences 112*, 839-844.

Chapter V

A two-component micelle with emergent pH responsiveness by mixing dilauroyl phosphocholine and deoxycholic acid and its delivery of proteins into the cytosol

V-1 Introduction

Drug-delivering nanoparticles are nanomachines or nanovehicles for transporting therapeutic agents into the targeted site in biological systems. Such nanoparticles are constructed by polymeric materials, lipids, or even biocompatible inorganic materials. When the target site is located inside cells, which is the case for antigen proteins (or peptides) and therapeutic nucleotides, endosomal escape, namely, the evasion of lysosomal trapping and degradation to promote release of the cargo into the cytosol [1], is one of the most important functions for a drug delivery system (DDS). Many nanoparticles have been designed to achieve this. Several chemical functional groups, including peptides to form pores on the endosomal membrane, protonatable groups to induce a pH-buffering effect, and a functional group to induce fusion into the endosomal bilayer, have been proposed to facilitate endosomal escape [2]. Among these alternatives, polycations such as polyethylenimine and poly(L-lysine) have been used, with the expectation that they have a certain pH-buffering effect, called the "proton sponge hypothesis" [3]. Since amines in these polymers are basic (pKa is 8-9), they can absorb the protons while avoiding the acidification of endosome; as protons are coming with Cl-, which is hydrated, the influx of Cl- and associated water ruptures the endosomes, which finally causes release of its cargo into the cytosol. The proton sponge hypothesis has been challenged because of a lack of concrete experimental evidence [4]. Although the proton sponge effect may not be a correct mechanism, it is clear that pH-responsive nanoparticles are still a major factor in transporting cargo to intracellular targets. The target of pH-responsive nanoparticles is not only the cytosol, but also around cancer's environment[5]. Several pathological conditions, including cancer, ischemic stroke, inflammation, and atherosclerotic plaques, are related to metabolic activity and hypoxia, leading to decreasing pH in the vicinity[6]. Therefore, these sites

can be other major targets of pH-responsive DDS. Recently, Maeda et al. proposed an effective DDS for pirarubicin (or 4′-O-tetrahydropyranyl adriamycin) by combining the enhanced permeability and retention effect and a pH-responsive imine bond [7].

Many pH-responsive nanoparticles have been reported for DDS applications. Among them, cationic lipids after mixing with helper lipids, such as dioleoyl-phosphatidylethanolamine (DOPE) or cholesterol, are normally used. The effects of DOPE on destabilizing endosomal membranes and mediating endosomal escape have been discussed in many papers [8,9] and books [10]. The potential for the cargo to be released into the cytosol means that many biological events can be induced. As one example, when protein antigens were the cargo, a fragmented peptide-MHC I complex stimulated CD8$^+$ T cells and a cellular immune response including cytotoxic T lymphocyte activity, which is the most important event in cancer immunotherapy. In the case of therapeutic oligonucleotides such as antisense DNA and siRNA, silencing of the specific gene that is targeted by the oligonucleotides would occur. Our previous work showed that the pH-responsive range for inducing a structural transition of the nanoparticles strongly depends on the DOPE content and, when its transition pH matches the pH at which a change from early to late endosome occurs, the delivery efficiency reaches its maximum. Although DOPE-containing liposomes have been shown to be quite effective in some *in vitro* systems [10,11], *in vivo* study is different. It has been reported that DOPE causes unfavorable side effects including savior toxicity in organs and cells [12]. Many other studies have adopted a similar pH-responsive strategy in designing nanoparticles [13,14]. In most of these studies, a new material or functional group was attached to provide the pH responsiveness. Although these worked adequately, new materials are sometimes associated with safety issues, so there would be a larger barrier to fulfill legal requirements for medical usage.

Sakaguchi et al. established a new pH-responsive nanoparticle made from dilauroyl phosphocholine (DLPC) and deoxycholic acid (DA) [15]. Deoxycholic acid and its family, generally called bile acids, are known as typical steroid derivatives that are secreted from the gallbladder to emulsify dietary fats, fat-soluble vitamins, and other hydrophilic compounds. They are known as a controlling signal molecule for homeostasis, glycometabolism, lipid metabolism and energetic metabolism[16,17]. In the body, they play a role in promoting absorption, among others. Because of their origin, they are not associated with any serious toxicities[18]. Among the bile acids, DA and ursodeoxycholic acid have been approved as pharmaceutical additives for injection into humans [19]. In addition, DLPC is one of the major lipids constituting cellular membranes and has a rather long history of clinical use [20,21]. Therefore, the DLPC/DA system is expected not to have any issues regarding toxicity and unfavorable side effects. The aim of the present paper is to clarify the pH-responsive properties of this system and to understand its mechanism of action at the molecular level.

V-2 Experimental

2.1. Materials

Egg yolk phosphatidylcholine (EYPC; COATSOME NC-50 grade) and DLPC (COATSOME MC-1212 grade) were obtained from NOF Corporation. DA was obtained from Tokyo Chemical Industry Co., Ltd. Ovalbumin-conjugated fluorescein (F-OVA) was purchased from Invitrogen (Carlsbad, CA, USA). Lyso Tracker® Red Lysosomal Probe was purchased from Lonza Walkersville, Inc. (Walkersville, MD, USA). The preparation of the DLPC/DA micelles was described in a preceding patent application, but it can be briefly summarized as follows: 1000 nM DLPC was dissolved in methanol and DA was also dissolved in methanol. After mixing them at a given ratio,

the solvent was evaporated. MES buffer (MES: 25 mM, NaCl: 125 mM, pH 7.4) was added after evaporation and dispersed using ultra-sonication.

2.2. Characterizing pH responsiveness: interaction with a model membrane:

In accordance with a previously reported method, the nanoparticle/liposome membrane interaction was examined. First, we prepared an EYPC liposome encapsulating pyranine as a fluorescent dye, with controlled sizes (*ca.* 100 nm) using a polycarbonate film with a pore size of 100 nm. After the outer water layer had been substituted by an MES buffer (MES: 25 mM, NaCl: 125 mM, pH 7.4), we added a nanoparticle solution and adjusted the final pH. The final concentration of DLPC and DA were 6.67 μM and 1.07 μM, respectively. The leakage of pyranine was monitored with a fluorescence spectrometer (Jasco Co., Tokyo, Japan) .

2.3. Dynamic light scattering

The zeta potential (ζ) and the hydrodynamic radius (R_h) were determined for the samples in a HEPES buffer (HEPES: 1.0 mM) whose pH was adjusted to 7.4 with a Nano ZS 90.

2.4. Synchrotron small-angle X-ray scattering (SAXS)

The SAXS measurements were performed at BL-40B2 of SPring-8, Japan. A 30 × 30 cm imaging plate (Rigaku R-AXIS VII) detector was placed 1.65 m from the sample [22]. The wavelength of the incident beam (λ) was 0.10 nm. A bespoke SAXS vacuum sample chamber [23] was used and the X-ray transmittance of the samples was determined with an ion chamber located in front of the sample and a Si photodiode for X-rays (Hamamatsu Photonics S8193) behind the sample. The sample concentration was 1 mM in 150 mM NaCl and the exposure time was 300 s for all measurements. The scattering intensity $I(q)$ was measured as a function of the scattering angle of 2θ and 2θ was

converted to the magnitude of the scattering vector (q) using the equation $q = (2\pi/\lambda)\sin\theta$.

2.5. Cytosolic delivery of ovalbumin-conjugated fluorescein (F-OVA) into RAW264.7 cells

RAW264.7 cells were purchased from American Type Culture Collection (Manassas, VA, USA) and cultured in Dulbecco's modified Eagle's medium (DMEM) (Wako Pure Chemical Industries, Ltd., Osaka, Japan) at 37°C in 5% CO_2. F-OVA was dissolved in phosphate-buffered saline (PBS). DLPC/DA or EYPC/DA with F-OVA at 5.0 μg/mL was added to 2×10^5 cells per six-well plate. After 3 h, the cells were washed twice with PBS, stained with Lyso Tracker® Red Lysosomal Probe, in accordance with the manufacturer's protocols, and a cellular image was obtained by confocal microscopy (Nikon Co., Tokyo, Japan).

V-3 **Results and Discussions**

Mixing behavior of DLPC/DA

Figure 2A shows how the appearance of the solution changed upon the addition of DA to DLPC, when the solution's pH was kept at 7.4 by using MES buffer. DLPC itself did not form a stable spherical micelle. According to previous work [24,25], it forms vesicles, more precisely multilayered vesicles, and its size can become comparable with the visible lights. Therefore, these vesicles in solution exhibit turbidity. Upon adding DA, the turbidity decreased and the solution became transparent at $\varphi = 0.28$, where φ is defined by the molar composition ratio of $\varphi = [DA]/([DA] + [DLPC])$. This change in appearance suggests that the addition of DA decreased the size of aggregates of DLPC and DA. This feature is more clearly confirmed by the DLS data shown in Figure 2B, where the auto-correlation functions are compared with the different compositions. With an increase of φ, the initial slope decreased drastically. By using the software supplied by Malvern, R_h was determined, as plotted in Figure 2C. R_h decreased and reached to $R_h < 10$ at $\varphi = 0.3$ and to a plateau at $\varphi > 0.6$. The software was used to calculate the polydispersity dispersity index (PDI) for R_h and PDI became smaller with an increase of DA. Figure 2C also presents the change in zeta potential, indicating that ζ reaches about -30 mV at $\varphi > 0.62$. Its negative charge is due to the carboxylic group of the DA acid. At $\varphi > 0.6$, the majority is DA acid and thus we assume that the negatively charged carboxylic group covers the surface of the nanoparticle. Hereinafter, we set $\varphi = 0.62$ and confirmed that, when the composition was in the range of $\varphi > 0.6$, there were no major differences in the rest of the measurements[15]. Table 1 compares the values of R_h, PDI, and ζ.

Figure 3 illustrates the structural transition that occurred when DA was added to DLPC.

DLPC forms multilayered vesicles[25], which was confirmed for our system with SAXS, showing the typical inter-layer diffraction at $q = 1.08$ and $2.15\,\text{nm}$ (see Supplementary Figure 1). Upon adding DA to DLPC, R_h drastically decreased and the diffraction peaks disappeared at $\varphi > 0.5$ (data not shown). This means that the addition of DA induced the transition from vesicles to spherical micelles. According to the packing parameter principle [26], to shift from a vesicle to a spherical micelle, it is necessary to increase the volume fraction of the hydrophilic group compared with the hydrophobic tail length and volume. Therefore, we assume that the added DA was trapped in the hydrophilic domain of the preceding DLPC vesicle and increased the domain volume. From the finding that the addition of DA increased the negative ζ value, the ionized carboxylic group of DA might have faced the water phase while the steroid moiety of DA is located in the hydrophobic core. This ion pairing and the water affinity of the carboxylic group were dominant, so the steroid moiety of DA may not have become buried deep in the hydrophobic tail domain. Judging from the molecular size, the moiety may have been located near the interface. We suppose that the ion pairing between the OH group of the DA and the phosphoric group of the DLPC may have helped to stabilize the presence of the relatively hydrophobic steroid moiety in the

hydrophilic domain. The ionized carboxylic group of DA was confirmed by infrared

spectroscopy (see the supplementary information).

pH-responsive membrane disruption

Figure 4A presents that pH dependence of the pyranine leakage from a giant EYPC

liposome when DLPC/DA micelles were mixed. The negative controls (each individual

component): DA, DLPC, and EYPC showed no leakage under all pH conditions. Even

in the case of EYPC/DA, no leakage was shown. Only when we added a mixture of DA

and DLPC at $\varphi = 0.62$ was leakage clearly observed at pH < 6. Figure 4B shows the

pH-leakage plots for other bile acids: chenodeoxycholic (CDA) and ursodeoxycholic

acids (UDA); as shown by the chemical structures in the figure, the only difference

between these two compounds is in the chirality of the OH groups at the 3 and 7

positions, while neither has the position 12 OH. Figure 4B indicates that the

stereochemistry of the OH groups at the 3 and 7 positions provides a drastic change in

the pH responsiveness in the leakage, only when mixed with DLPC. Pierrat et al.

reported that the pKa of ionizable lipids are influenced by coexisting other lipids when

they are mixed. This pKa shift is caused by lipid-lipid interactions, including that the

presence of a long hydrophilic spacer between the hydrophobic part of the ionizable

lipids and the other polar head changes the distance between the heads of the ionizable

lipids [27]. Similarly to this result, the apparent pKa values of CDA and UDA in the

mixed states may change according to the difference in stereochemistry between CDA

and UDA. Figure 4C shows the dependence of the pH responsiveness on the alkyl chain

length (n), where n stands for the carbon number in the phosphatidylcholine lipid family,

as shown in the figure. When n was greater than 14, no leakage was observed, while at

$n = 10$, leakage was observed at both pH 7.4 and 5.0; that is, there was no pH

responsiveness. These results suggest that the pH responsiveness of the dual-lipid mixtures may have emerged due to the combination of the hydrophobic interaction in the alkyl domain and the interactions between the DLPC headgroup and the bile acid, created by the position and stereochemical effect of the OH groups in the bile acids.

Delivery to the cytosol using the DLPC/DA system

We examined how much F-OVA is transferred into the cytosol upon co-administering F-OVA and DLPC/DA to RAW264.7 cells (Figure 5). Lysosomes and late endosomes are labeled red by the Lyso Tracker probe [28]. After overlaying the red and green (from F-OVA) images, DLPC/DA showed a large amount of separation between these two colors, while EYPC/DA exhibited an orange color in most areas, meaning that the ingested F-OVA was localized at lysosomes. Upon careful examination of the distribution of the green color, it appeared to be spread throughout the cell interior, but with some still confined to the lysosomes. This experiment demonstrates that DLPC/DA provides more cytosolic release of F-OVA than EYPC/DA. This difference corresponds to the pH-responsive leakage shown in Figure A. Therefore, we assume that the pH responsiveness of DLPC/DA induces the release of F-OVA into the cytosol.

It should be noticed that there is no interaction between F-OVA (also OVA) and the lipids, and they keep free in solution (see the supplementary). Our delivering system is designed for vaccination to transfer antigen proteins as well as adjuvants to immunocytes. Normally, these vaccines are administrated through subcutaneous or intramuscular injection. In these cases, the injected materials tend to stay at the same part or be transported to lymphnodes then, eventually engulfed by macrophages or DCs [29,30]. Their local concentrations can be kept relatively high during a certain period and there may be a large possibility to be simultaneously ingested. Therefore, it is not necessary to bind antigen proteins and pH-responsive particles.

Micellar structural changes observed by SAXS

Figure 6 shows the pH dependence of the SAXS profiles of DLPC/DA. At pH 7.0 and 6.5, the low q intensity satisfies the relationship $I(q) \propto q^{\alpha}$ with $\alpha = 0$, and there is a sharp intensity minimum at $q = 1.0 \text{ nm}^{-1}$; this value is denoted as $q_{1\text{st min}}$. These features indicate the formation of spherical micelles from DLPC/DA, with a rather narrow size distribution; otherwise, no minimum would be observed. When the scattering object is a solid sphere with a radius of R (i.e., a sphere with uniform electron density and a sharp interface with the solvent), $R \times q_{1\text{st min}} \sim 4.5$. This suggests that the diameter of the micelle is approximately 9 nm, which is consistent with the DLS result in Table 1. We attempted to fit the SAXS profiles at pH 7.0 and 6.5 with a simple model, such as a solid sphere or a core-shell double-layer model, but could not obtain a reasonable fit. This may have been due to the complex structure of interaction between the hydrophilic headgroup of DLPC and DA.

With an increase of pH, the scaling factor α at low q changes from $\alpha = 0$ to $\alpha = -1.2$ to -2.0 [31]. This change can be interpreted in two ways: (i) structural transition from sphere to vesicle or plate or (ii) aggregation of preceding spheres. If a structural transition takes place, $q_{1\text{st min}}$ would change, but this is not the case in the present system. Therefore, we suppose that the change of α is related to aggregation. The start of aggregation means that the surface of the micelles becomes less water-compatible or hydrophilic. This could be related to protonation of the carboxylic group or induced changes between DLPC and DA. Therefore, we can conclude that decreasing pH leads to an increase of H^+, which increases the population of COOH instead of COO^-. This directly decreases the hydrophilicity of the micellar surface and/or changes the nature of molecular interactions, most likely hydrogen bonding between DLPC and DA. This causes secondary aggregation between the micelles.

Furthermore, inter-micellar hydrogen bonding can occur through the surface COOH groups, which also facilitates the formation of aggregates.

Proposing a mechanism of the pH responsiveness of DLPC/DA and its delivery of proteins to the cytosol

When DLPC and DA are mixed at an appropriate ratio, the resultant mixture shows the emergent property of pH responsiveness. The pH response range is mainly determined by the position and stereochemistry of OH groups in DA and its sensitivity (in terms of the leakage test) is related to the hydrophobicity of the alkyl chain of DLPC. The pH responsiveness is related to a reduction of hydrophilicity on the micellar surface. Based on these results, we can speculate the enhanced efficiency in the protein delivery with DLPC/DA system as follows (Figure 7). After DLPC/DA and proteins are ingested by endocytosis, the pH of the endosomal vesicle decreases in the late stage. This pH change reduces the hydrophilicity of the nanoparticle surface and the particle becomes unstable, which leads to aggregation. The endosomal compartment is a spatially confined region, and thus the unstable particles may attach to the vesicle bilayers. In this process, fusion may occur, leading to the mixing or merging of DLPC and/or DA into the bilayers. These events may destabilize the endosomal vesicle and eventually lead to its rupture, similar to that leading to leakage of the cargo of giant EYPC vesicles. It should be noted that this pH responsiveness only occurs when DLPC and DA are mixed.

V-4 Conclusions

The pH responsiveness that emerged for the mixture of DLPC and bile acid is a novel and interesting finding. Although the molecular mechanism behind this phenomenon has not been completely clarified, the pH response range can be adjusted by changing the chemical structure of the bile acid. In terms of safety, both DLPC and bile acids are approved as drug materials by the FDA, which reduces the burden in new drug development. As our protein delivery assay showed, DLPC/DA can transport co-administered materials into the cytosol. This property may be useful for a broad range of applications, including antigen-protein delivery[32], cancer immunotherapy or for therapeutic oligonucleotide delivery, including micro-RNA, siRNA, and antisense DNA.
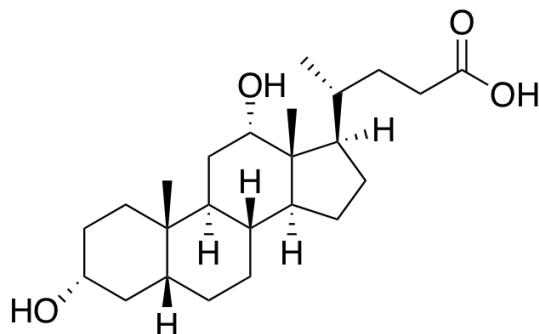
V-5 Table and Figures

Table 1. The diameters and zeta potentials of DLPC and DLPC/DA.

|	DLPC	DLPC/DA
Diameter (nm)	350	12
PDI	0.55	0.16
Zeta potential (mV)	-2.3	-30
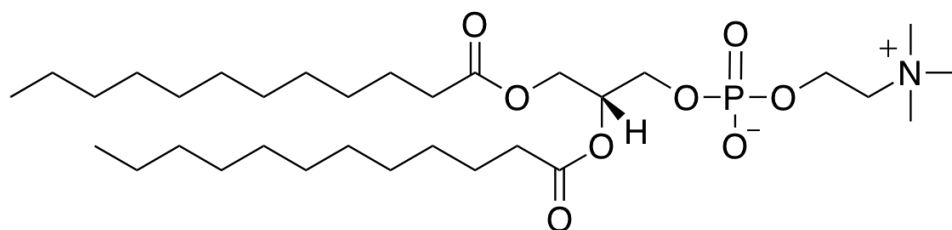
1,2-dilauroyl-sn-glycero-3-phosphocholine or **dilauroyl phosphocholine** (DLPC)


4-((3*R*, 5*R*, 8*R*, 9*S*, 10*S*, 12*S*, 13*R*, 14*S*, 17*R*)-3,12-dihydroxy-10,13-dimethylhexadecahydro-1*H*-cyclopenta[*a*]phenanthren-17-yl)pentanoic acid or **deoxycholic acid (DA)**

Figure 1. Chemical structures of dilauroyl phosphocholine and deoxycholic acid.
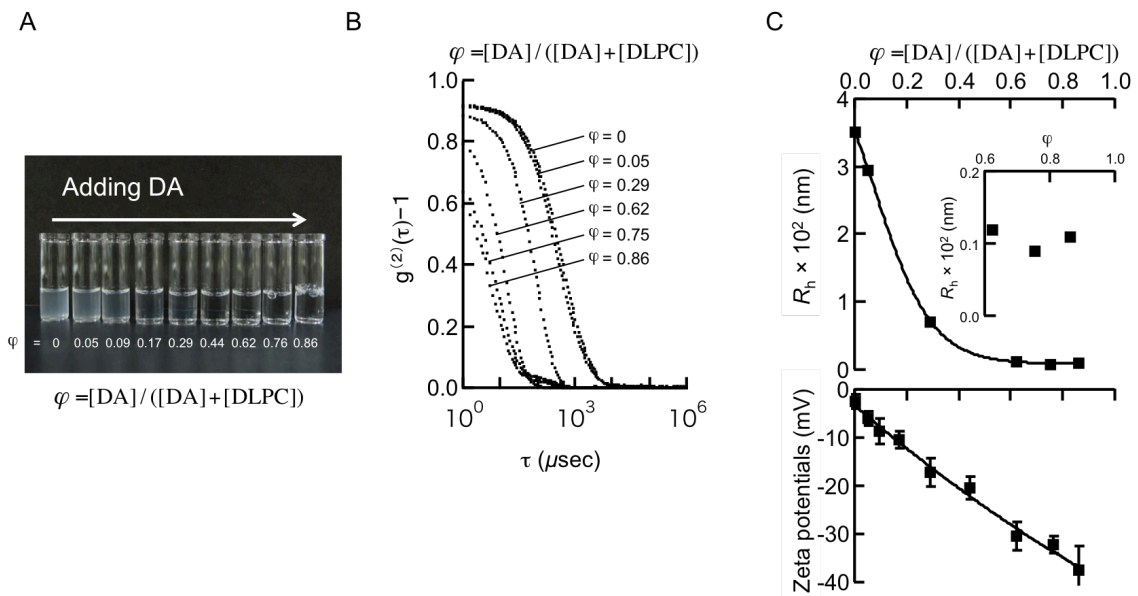
Figure 2. Composition (φ) dependence of the appearance of the DA and DLPC mixtures at pH 7.4 (A), and the auto-correlation functions measured with DLS (B), and the average hydrodynamic radius and the zeta-potential (C).
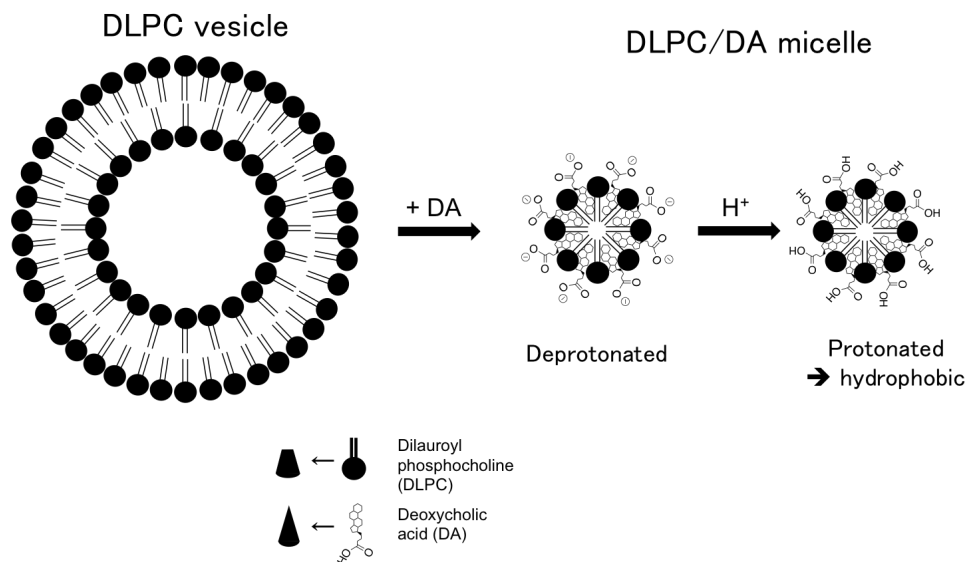
Figure 3. A schematic illustration of the structural transition from the DLPC vesicle to the DLPC/DA spherical micelle; lowering the pH leads to protonation of the carboxylic group. DLPC and DA can be represented by a cylinder (or a flat head cone) and a cone, respectively, in terms of the packing parameter principle and thus mixing the cone-shaped DA to the DLPC bilayer induces a structural transition to spherical shape. Decreasing pH leads protonation of the carboxyl group and thus becomes less hydrophilic or more favorable to form hydrogen bonds with the DLPC head group.
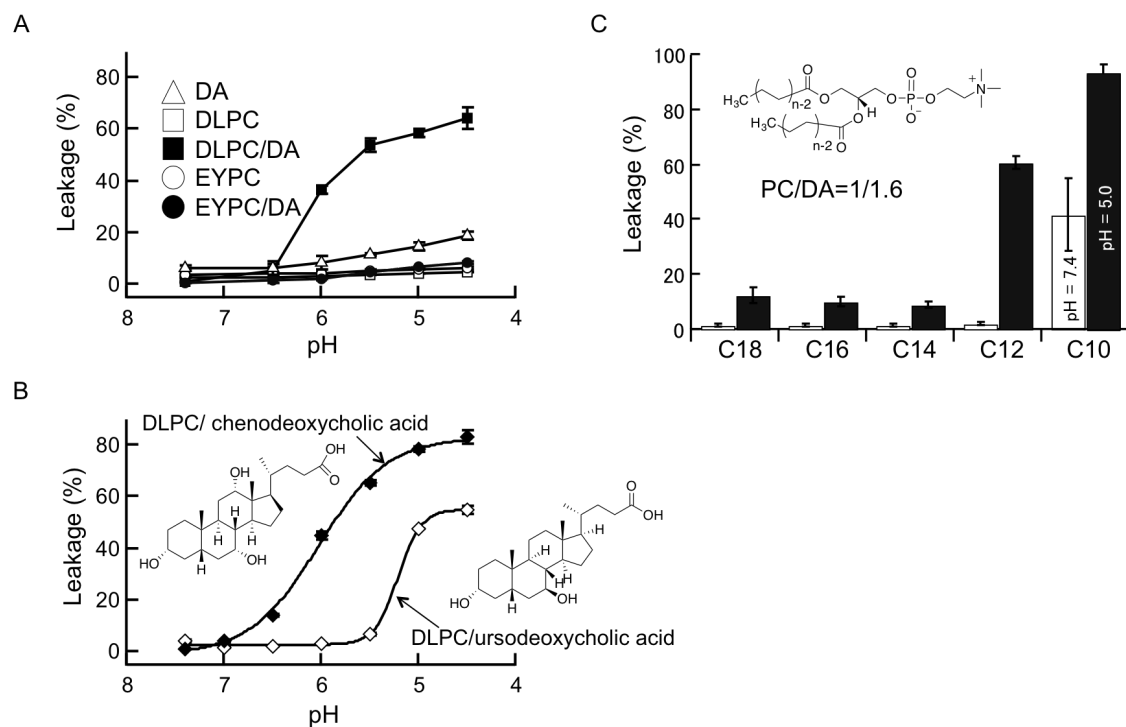
Figure 4. The leakage behavior for the dual-lipid micelles (DLPC/DA in panel A, and DLPC/chenodeoxycholic acid and DLPC/ursodeoxycholic acid in panel B) comparing their individual components and EYPC/DA, and the effect of the alkyl tail length in DLPC analogues on the pH responsiveness, showing that mixing with DLPC and a bile acid is necessary to induce pH responsiveness. The tail length dependence of the DLPC analogues.
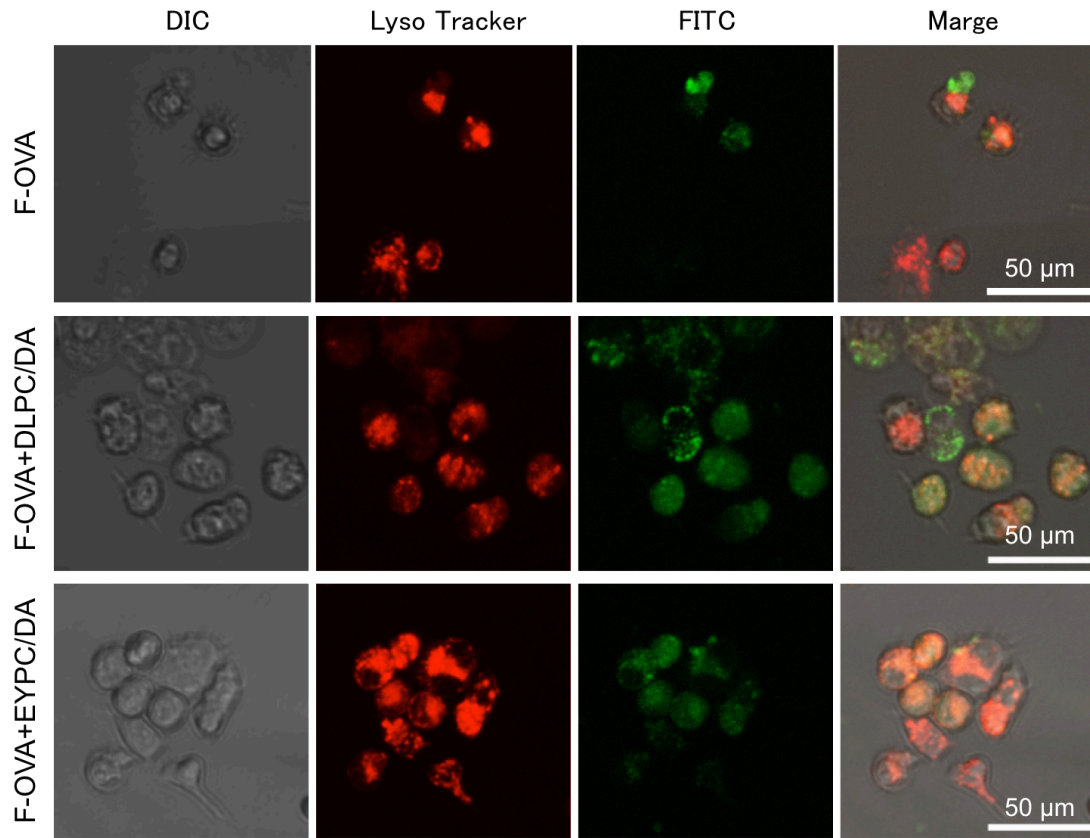
Figure 5. Confocal microscopic images upon co-administering only F-OVA and F-OVA and DLPC/DA to RAW264.7 cells, compared with those of F-OVA and EYPC/DA.
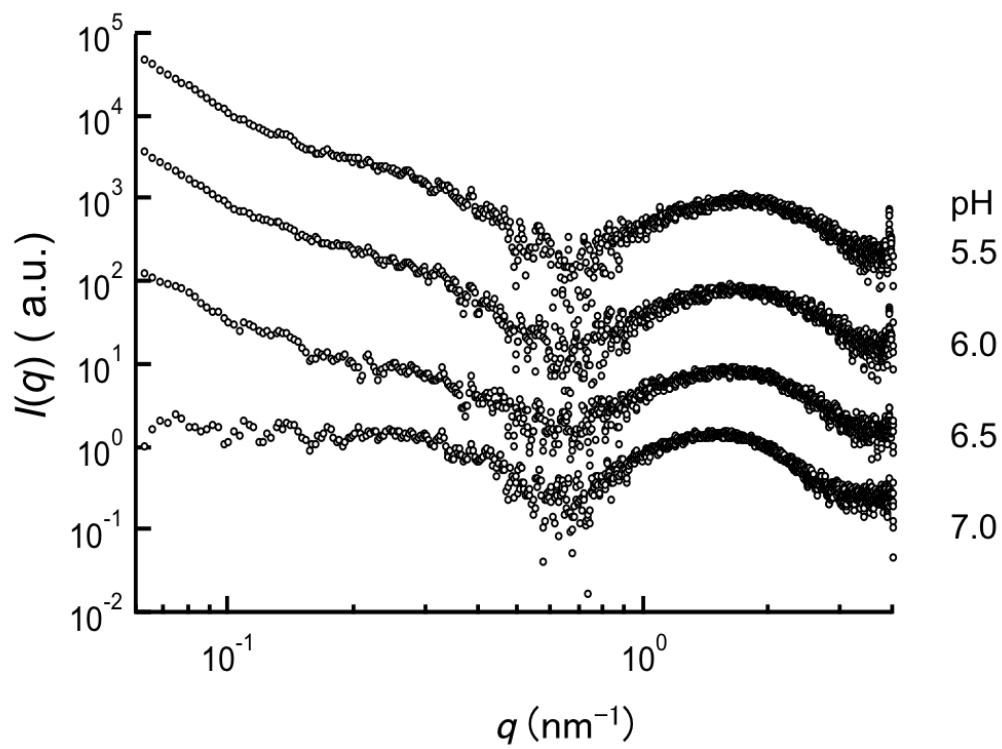
Figure 6. The pH dependence of SAXS profiles of DLPC/DA.
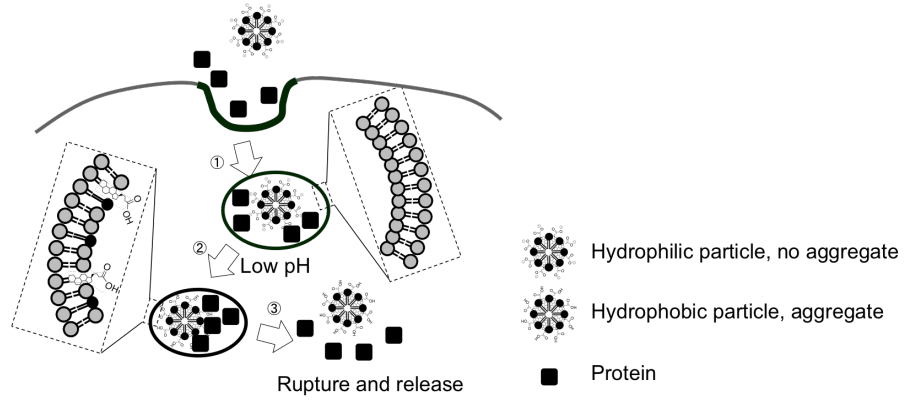
Figure 7. A schematic illustration of the protein delivery with the DLPC/DA system, when they are co-administrated (see the text in detail).

Supplementary Figure
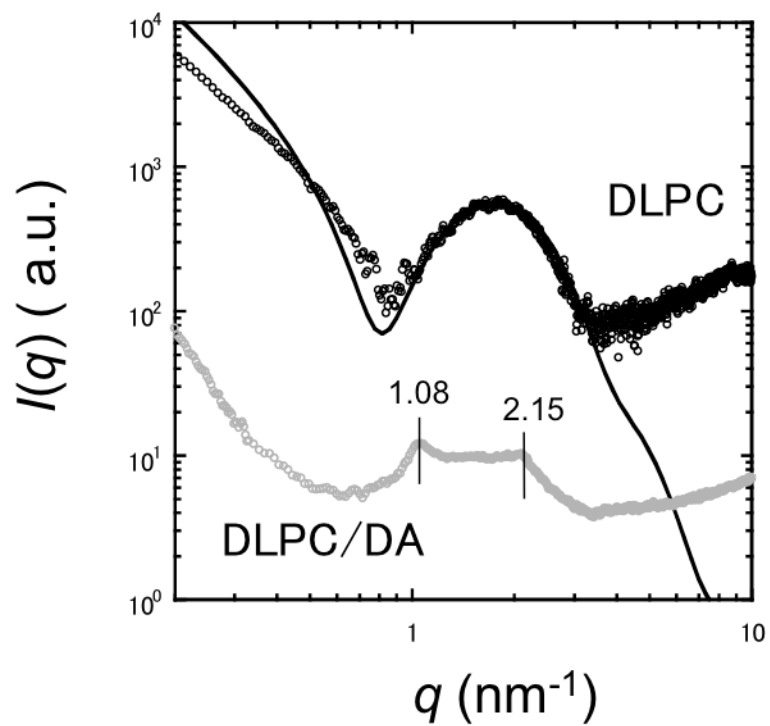
Supplementary Figure 1. Typical inter-layer diffraction of DLPC (black) and DLPC/DA (gray)
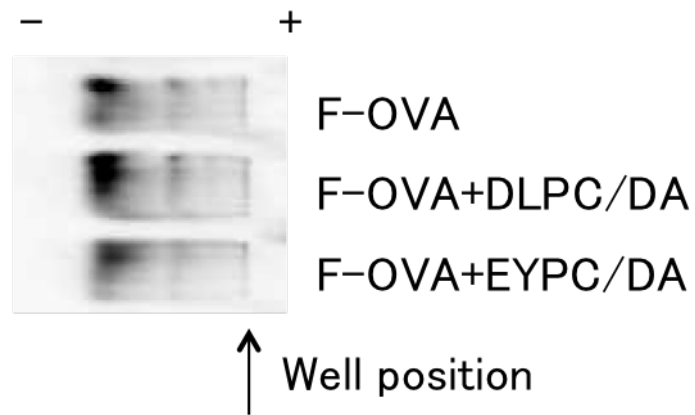
Supplementary Figure 2. The mixture of F-OVA and DLPC/DA. The fluoresense of F-OVA was observed after migration at 30 min to 12 wt % acrilamidegel electrophoresis.

V-6 References

(1)   Canton, I., and Battaglia, G. (2012) Endocytosis at the nanoscale. *Chem Soc Rev 41*, 2718-2739.

(2)   Varkouhi, A. K., Scholte, M., Storm, G., and Haisma, H. J. (2011) Endosomal escape pathways for delivery of biologicals. *Journal of Controlled Release 151*, 220-228.

(3)   Behr, J.-P. (1997) The Proton Sponge: a Trick to Enter Cells the Viruses Did Not Exploit. *CHIMIA International Journal for Chemistry 51*, 34-36.

(4)   Benjaminsen, R. V., Mattebjerg, M. A., Henriksen, J. R., Moghimi, S. M., and Andresen, T. L. (2013) The possible "proton sponge " effect of polyethylenimine (PEI) does not include change in lysosomal pH. *Mol Ther 21*, 149-157.

(5)   Gao, W., Chan, J. M., and Farokhzad, O. C. (2010) pH-responsive nanoparticles for drug delivery. *Molecular pharmaceutics 7*, 1913-1920.

(6)   Gao, W., Chan, J. M., and Farokhzad, O. C. (2010) pH-Responsive nanoparticles for drug delivery. *Mol Pharm 7*, 1913-1920.

(7)   Maeda, H., Tsukigawa, K., and Fang, J. (2016) A Retrospective 30 Years After Discovery of the Enhanced Permeability and Retention Effect of Solid Tumors: Next-Generation Chemotherapeutics and Photodynamic Therapy--Problems, Solutions, and Prospects. *Microcirculation 23*, 173-182.

(8)   Wasungu, L., and Hoekstra, D. (2006) Cationic lipids, lipoplexes and intracellular delivery of genes. *J Control Release 116*, 255-264.

(9)   Mochizuki, S., Kanegae, N., Nishina, K., Kamikawa, Y., Koiwai, K., Masunaga, H., and Sakurai, K. (2013) The role of the helper lipid

dioleoylphosphatidylethanolamine (DOPE) for DNA transfection cooperating with a cationic lipid bearing ethylenediamine. *Biochimica et biophysica acta 1828*, 412-418.

(10)   Philippot, J. R., and Schuber, F. (1994) *Liposomes as tools in basic research and industry*, CRC press.

(11)   Huang, L., Hung, M. C., and Wagner, E. (1999) *Nonviral Vectors for Gene Therapy*, Academic Press, London, UK.

(12)   Lv, H., Zhang, S., Wang, B., Cui, S., and Yan, J. (2006) Toxicity of cationic lipids and cationic polymers in gene delivery. *Journal of Controlled Release 114*, 100-109.

(13)   He, Q., Gao, Y., Zhang, L., Zhang, Z., Gao, F., Ji, X., Li, Y., and Shi, J. (2011) A pH-responsive mesoporous silica nanoparticles-based multi-drug delivery system for overcoming multi-drug resistance. *Biomaterials 32*, 7711-7720.

(14)   Hoffman, A. S. (2013) Stimuli-responsive polymers: Biomedical applications and challenges for clinical translation. *Advanced Drug Delivery Reviews 65*, 10-16.

(15)   Sakaguchi, N. (2016), US 9248192 B2.

(16)   Morimoto, K., Itoh, H., and Watanabe, M. (2013) Developments in understanding bile acid metabolism. *Expert Review of Endocrinology & Metabolism 8*, 59-69.

(17)   Kuipers, F., Bloks, V. W., and Groen, A. K. (2014) Beyond intestinal soap[mdash]bile acids in metabolic control. *Nat Rev Endocrinol 10*, 488-498.

(18)   Hofmann, A., and Hagey, L. (2008) Bile acids: chemistry, pathochemistry,

biology, pathobiology, and therapeutics. *Cellular and Molecular Life Sciences 65*, 2461-2483.

(19)   Ganley, D. J., and Wilt, J. (2013), 206333

(20)   Saari, M., Vidgren, M. T., Koskinen, M. O., Turjanmaa, V. M., and Nieminen, M. M. (1999) Pulmonary distribution and clearance of two beclomethasone liposome formulations in healthy volunteers. *International journal of pharmaceutics 181*, 1-9.

(21)   Taira, K., Kataoka, K., and Niidome, T. (2014) *Non-viral gene therapy*, Springer.

(22)   Masunaga, H., Sasaki, S., Tashiro, K., Hanesaka, M., Takata, M., Inoue, K., Ohta, N., and Yagi, N. (2007) Development of Synchrotron DSC/WAXD/SAXS Simultaneous Measurement System for Polymeric Materials at the BL40B2 in SPring-8 and its Application to the Study of Crystal Phase Transitions of Fluorine Polymers. *Polymer Journal 39*, 1281-1289.

(23)   Naruse, K., Eguchi, K., Akiba, I., Sakurai, K., Masunaga, H., Ogawa, H., and Fossey, J. S. (2009) Flexibility and Cross-Sectional Structure of an Anionic Dual-Surfactant Wormlike Micelle Explored with Small-Angle X-ray Scattering Coupled with Contrast Variation Technique. *The Journal of Physical Chemistry B 113*, 10222-10229.

(24)   Kučerka, N., Liu, Y., Chu, N., Petrache, H. I., Tristram-Nagle, S., and Nagle, J. F. (2005) Structure of Fully Hydrated Fluid Phase DMPC and DLPC Lipid Bilayers Using X-Ray Scattering from Oriented Multilamellar Arrays and from Unilamellar Vesicles. *Biophysical Journal 88*, 2626-2637.

(25)   Danila, D. C., Banner, L. T., Karimova, E. J., Tsurkan, L., Wang, X., and Pinkhassik, E. (2008) Directed Assembly of Sub-Nanometer Thin Organic Materials with Programmed-Size Nanopores. *Angewandte Chemie International Edition 47*, 7036-7039.

(26)   Israelachvili, J. N. (1992) *Intermolecular and surface forces*, Vol. 450, Academic press London.

(27)   Pierrat, P., and Lebeau, L. (2015) Characterization of Titratable Amphiphiles in Lipid Membranes by Fluorescence Spectroscopy. *Langmuir 31*, 12362-12371.

(28)   Chazotte, B. (2011) Labeling lysosomes in live cells with LysoTracker. *Cold Spring Harb Protoc 2011*, pdb prot5571.

(29)   Hailemichael, Y., Dai, Z., Jaffarzad, N., Ye, Y., Medina, M. A., Huang, X.-F., Dorta-Estremera, S. M., Greeley, N. R., Nitti, G., and Peng, W. (2013) Persistent antigen at vaccination sites induces tumor-specific CD8+ T cell sequestration, dysfunction and deletion. *Nature medicine 19*, 465-472.

(30)   Kobiyama, K., Aoshi, T., Narita, H., Kuroda, E., Hayashi, M., Tetsutani, K., Koyama, S., Mochizuki, S., Sakurai, K., and Katakai, Y. (2014) Nonagonistic Dectin-1 ligand transforms CpG into a multitask nanoparticulate TLR9 agonist. *Proceedings of the National Academy of Sciences 111*, 3086-3091.

(31)   Roe, R.-J. (2000) *Methods of X-ray and neutron scattering in polymer science*, Vol. 739, Oxford University Press on Demand.

(32)   Sakaguchi, N. (2016), US2016271246 A1.

124

Chapter VI

Summary and Conclusions

In this thesis we have explored the drug delivery system of CpG-ODN into SPG for cancer vaccine, cytosol delivery with cell penetrating peptide into SPG, and characterization of pH responsiveness micelle. The following summarized the results obtained in each chapter.

Preparation and characterization of crosslinking(CL)-CpG complex (Chapter II)

β-Glucan schizophyllan (SPG) and CpG-dA40 can form a complex (CpG-dA40/SPG), which drastically induces immune-response owing to a combination of immunocyte-targeting delivery due to SPG and immunostimulative CpG ODN. We made a crosslinked larger particle than the original one by using hybridization. The crosslink particles showed higher immune stimulation and can thus be used as a more potent vaccine adjuvant than CpG-dA40/SPG itself.

Approach as a Cancer vaccination with CL-CpG (Chapter III)

Cancer vaccine has an ability to directly eradicate tumor cells by creating and activating cytotoxic T lymphocytes (CTLs). To achieve efficient CTL activity and to induce Th1 responses, it is essential to administer an appropriate adjuvant as well as an antigen. CpG-ODN is known as a ligand of Toll-like receptor 9 (TLR9) and strongly induces Th1 responses. In our previous study, we developed a CpG-ODN delivery system by use of the formation of complexes between ODN and a beta-glucan SPG, denoted CpG/SPG, and demonstrated that CpG/SPG induces high Th1 responses. In this study, we created a nanogel made from CpG/SPG complexes through DNA-DNA hybridization [crosslinked (CL)-CpG]. Immunization with CL-CpG induced much stronger antigen-specific Th1 responses in combination with the antigenic protein ovalbumin (OVA) than that with CpG/SPG. Mice pre-immunized with CL-CpG and OVA exhibited a long delay in tumor growth and an improved survival rate after tumor

inoculation. These immune inductions can be attributed to the improvement of cellular uptake by the combination of increased size and the cluster effect of the beta-glucan recognition site in the nanogel structure. In other words, the particle nature of CL-CpG, instead of the semiflexible rod conformation of CpG/SPG, enhanced the efficacy of a cancer vaccine. The present results indicate that CL-CpG can be used as a potent vaccine adjuvant for the treatment of cancers and infectious diseases.

Cytosol delivery by using cell penetrating peptide with SPG (Chapter IV)

Antisense-oligonucleotides (AS-ODNs) are not able to protect the bound ODN against degradation enzyme in biological fluids and be taken up by targeting cells. To solve these issues, the development of drug delivery systems to deliver AS-ODNs has been studied.

We have studied a polysaccharide schizophyllan (denoted by SPG), a member of β-glucans, as a delivery carrier of oligonucleotides. SPG can form a complex with polydeoxyadenosine (denoted by dA base numbers) and prevents degradation by enzymes. We have reported that the complex comprising of SPG and the dA40 that was beforehand connected with AS-ODNs (AS-ODN-dA40). The complex can deliver AS-ODNs to dectin-1-expresseing cell and silence mRNA, then, eventually suppress protein expressions.

TAT peptide: human immunodeficiency virus type 1 protein fragments is known one of the major arginine-rich cell penetrating peptides. We prepared TAT peptide conjugate phosphorothioate dA40 oligonucleotide (denoted by TAT-dA40) by the click chemistry reaction. The TAT-dA40/ASHER3/SPG complexes showed a higher cell uptake and more cell-growth suppression than AS-yb-1-dA40/SPG complex that had not TAT. We suppose that this improvement can be ascribed to TAT-induced cellular ingestion of the

complexes.

pH responsiveness carrier and cytosol delivery(Chapter V)

Providing appropriate pH responsiveness for drug delivery nanoparticles is one of the major issues in developing a new generation of delivery systems. This paper reports that, when phosphocholine and a bile acid were mixed, the resultant two-component micelle gained pH responsiveness, while the individual components did not show any such responsiveness. The pH responsiveness was shown to be determined by the chemical structure, especially the positions and chirality of the OH groups, of the bile acid, and the sensitivity was determined by the alkyl chain length of the phosphocholine. The best combination for evading endocytosis was dilauroyl phosphocholine (DLPC) and deoxycholic acid (DA). Small-angle X-ray scattering revealed that the pH responsiveness was related to the change of surface hydrophobicity, namely, decreasing pH led to protonation of the carboxylic acid, resulting in aggregation of the preceding micelles. We assume that particles that become hydrophobic in this way can start interacting with the endocytotic bilayer, which eventually leads to rupture of the endocytotic vesicle. This mechanism is well supported by the finding that fluorescein-conjugated ovalbumin proteins were transported into the cytosol when they were co-administered with DLPC/DA.

Chapter VII

The Philosophy of This Research

Research is a creature and changes with the times.

The mature it teaches and gives me all things. Occasionally it teaches life and to touch a lot of contribution and knowledge of many giant. On the other hand, the immature it gives me curiousness and to research opportunity.

I would like to take part world medical as a researcher at long time. And I would like to be a researcher to form my curious and interesting.

In this Ph.D. student era, I thought such an above.

List of publications

Doctoral Thesis Publication

Chapter II

N. Miyamoto, S. Mochizuki, K. Sakurai, Enhanced Immunostimulation with Crosslinked CpG-DNA beta-1,3-Glucan Nanoparticle through Hybridization, Chemistry Letters 43(7) (2014) 991-993.

Chapter III

Miyamoto, N., Mochizuki, S., Fujii, S., Yoshida, K., and Sakurai, K. (2016) Adjuvant activity enhanced by crosslinked CpG-oligonucleotides in beta-glucan nanogel and its anti-tumor effect. Bioconjugate Chemistry.

Chapter IV

Maegawa, Y., Mochizuki, S., Miyamoto, N., and Sakurai, K. (2016) Gene silencing using a conjugate comprising Tat peptide and antisense oligonucleotide with phosphorothioate backbones. Bioorganic & medicinal chemistry letters 26, 1276-1278.

Chapter V

Miyamoto, S., Fujii, N., Sakaguchi, S., Mochizuki, and K., Sakurai, A two-component micelle with emergent pH responsiveness by mixing dilauroyl phosphocholine and deoxycholic acid and its delivery of proteins into the cytosol (minor revision)

List of Publifications

1. First author

1-1. 宮本寛子、望月慎一、櫻井和朗、多糖 β-1,3 グルカンの受容体を利用したオリゴ核酸の選択的デリバリー, cellulose communications, vol. 19 , p12-16, No.1, 2012

1-2. N. Miyamoto, S. Mochizuki, K. Sakurai, Enhanced Immunostimulation with Crosslinked CpG-DNA beta-1,3-Glucan Nanoparticle through Hybridization, Chemistry Letters 43(7) (2014) 991-993.

1-3. Miyamoto, N., Mochizuki, S., Fujii, S., Yoshida, K., and Sakurai, K. (2016) Adjuvant activity enhanced by crosslinked CpG-oligonucleotides in beta-glucan nanogel and its anti-tumor effect. Bioconjugate Chemistry.

1-4. N. Miyamoto, S. Mochizuki, K. Sakurai, A two-component micelle with emergent pH responsiveness by mixing dilauroyl phosphocholine and deoxycholic acid and its delivery of proteins into the cytosol, Colloids and Surfaces B (2016) (minor revision)

2. Co-author

2-1. 前川善哉, 望月慎一, 宮本寛子, 櫻井和朗, β-1,3-グルカンを用いた薬物送達システムへの応用, TIGG (2013)

2-2. 田之畑大二郎, 真田雄介, 望月慎一, 宮本寛子, 櫻井和朗, 核酸 β -1,3-グルカン複合体の溶液物性, 高分子論文集, (2015)

2-3. Y. Maegawa, S. Mochizuki, N. Miyamoto, K. Sakurai, Gene silencing using a conjugate comprising Tat peptide and antisense oligonucleotide with phosphorothioate backbones, Bioorg Med Chem Lett 26(4) (2016) 1276-8.

2-4. N. Miyamoto, S. Mochizuki, S. Shinkai, K. Sakurai, Supramolecular wrapping by beta-1,3-glucans toward polysaccharide-based functional materials, Nova, (2016)

3. Books

3-1. 宮本寛子, 望月慎一, 櫻井和朗, 多糖 β-1,3 グルカンを用いた CpG 核酸の選択的デリバリー, ナノ学会会報, 第 12 巻, 第 2 号, p79-84 , (2014)

3-2. 宮本寛子, 望月慎一, 櫻井和朗, 糖鎖の 新機能開発・応用ハンドブック（第 7 編マテリアルサイエンスと糖鎖, (2014)

3-3. 長尾章平, 望月慎一, 宮本寛子, 櫻井和朗, 第 17 章 生体高分子をバイオベースマテリアルとして用いた遺伝子デリバリー, CMC, (2015)

3-4. 伊藤大貴, 宮本寛子, 望月慎一, 櫻井和朗, 多糖核酸複合体による核酸医薬デリバリー, CMC, (2016)

3-5. 伊藤大貴, 宮本寛子, 望月慎一, 櫻井和朗, 多糖類による核酸アジュバントのデリバリー技術, CMC, (2016)